MICROWAVE LABORATORY REPORT NO. 90-P-3

MICROWAVE ACTIVE FILTERS BASED ON COUPLED NEGATIVE RESISTANCE METHOD

TECHNICAL REPORT

CHI-YANG CHANG AND TATSUO ITOH

APRIL 1990

UNITED STATES ARMY RESEARCH OFFICE
CONTRACT NUMBER DAAL-03-88-K-005

TEXAS ADVANCED TECHNOLOGY PROGRAM

THE UNIVERSITY OF TEXAS AT AUSTIN
DEPARTMENT OF ELECTRICAL AND COMPUTER ENGINEERING
AUSTIN TEXAS 78712

REPORT DOCUMENTATION PAGE

1a. REPORT SECURITY CLASSIFICATION Unclassified	1b. RESTRICTIVE MARKINGS
2a. SECURITY CLASSIFICATION AUTHORITY	3. DISTRIBUTION / AVAILABILITY OF REPORT Approved for public release; distribution unlimited.
2b. DECLASSIFICATION / DOWNGRADING SCHEDULE	
4. PERFORMING ORGANIZATION REPORT NUMBER(S) Microwave Laboratory Report No. 90-P-2	5. MONITORING ORGANIZATION REPORT NUMBER(S) ARO 25045.39-EL
6a. NAME OF PERFORMING ORGANIZATION The University of Texas 6b. OFFICE SYMBOL (If applicable)	7a. NAME OF MONITORING ORGANIZATION U. S. Army Research Office
6c. ADDRESS (City, State, and ZIP Code) Dept. of Electrical & Computer Engineering Austin, Texas 78712	7b. ADDRESS (City, State, and ZIP Code) P. O. Box 12211 Research Triangle Park, NC 27709-2211
8a. NAME OF FUNDING / SPONSORING ORGANIZATION U. S. Army Research Office 8b. OFFICE SYMBOL (If applicable)	9. PROCUREMENT INSTRUMENT IDENTIFICATION NUMBER DAAL03-88-K-0005
8c. ADDRESS (City, State, and ZIP Code) P. O. Box 12211 Research Triangle Park, NC 27709-2211	10. SOURCE OF FUNDING NUMBERS PROGRAM ELEMENT NO. / PROJECT NO. / TASK NO. / WORK UNIT ACCESSION NO.

11. TITLE (Include Security Classification)
Microwave Active Filters Based on Coupled Negative Resistance Method

12. PERSONAL AUTHOR(S)
Chi-Yang Chang and Tatsuo Itoh

13a. TYPE OF REPORT	13b. TIME COVERED	14. DATE OF REPORT (Year, Month, Day)	15. PAGE COUNT
Technical	FROM _____ TO _____	1990, April	96

16. SUPPLEMENTARY NOTATION
The view, opinions and/or findings contained in this report are those of the author(s) and should not be construed as an official Department of the Army position policy, or decision, unless so designated by other documentation.

17. COSATI CODES		
FIELD	GROUP	SUB-GROUP

18. SUBJECT TERMS (Continue on reverse if necessary and identify by block number)
Microwave active filters, Negative resistance method, Active filters, Microwave filters

19. ABSTRACT (Continue on reverse if necessary and identify by block number)
Microwave active filters based on the coupled negative resistance method are investigated. The filter tank circuit unloaded Q value is increased to a value close to infinity using this design method. Therefore, filter passband performance improves significantly. A one-pole and a 2-pole narrowband active filter based on end-coupled filter structure are designed and fabricated. Based on the same structure, a one-pole and a 2-pole varactor tunable active filter are also built. A modified end-coupled filter is developed to broaden the bandwidth with a factor from 5 to 20 times. Based on this new structure, three 2-pole active filters with bandwidth from 1.75 percent to 7.5 percent are built. To broaden the filter bandwidth further, a modified parallel-coupled filter structure is introduced. Compared to the traditional parallel-coupled filter, this new structure has better upper stopband performance. The new structure is suitable for broadband active filters with a bandwidth up to 40 percent. All of the active filters described previously are suitable for microwave monolithic integrated circuit (MMIC) due to their planar structures. A none-pole MMIC fixed frequency active filter is designed.

20. DISTRIBUTION / AVAILABILITY OF ABSTRACT ☐ UNCLASSIFIED/UNLIMITED ☐ SAME AS RPT. ☐ DTIC USERS	21. ABSTRACT SECURITY CLASSIFICATION Unclassified
22a. NAME OF RESPONSIBLE INDIVIDUAL Tatsuo Itoh	22b. TELEPHONE (Include Area Code) (512) 471-1072 22c. OFFICE SYMBOL

ABSTRACT

Microwave active filters based on the coupled negative resistance method are investigated. The filter tank circuit unloaded Q value is increased to a value close to infinity using this design method. Therefore, filter passband performance improves significantly. A one-pole and a 2-pole narrowband active filter based on end-coupled filter structure are designed and fabricated. Based on the same structure, a one-pole and a 2-pole varactor tunable active filter are also built. A modified end-coupled filter is developed to broaden the bandwidth with a factor from 5 to 20 times. Based on this new structure, three 2-pole active filters with bandwidth from 1.75 percent to 7.5 percent are built. To broaden the filter bandwidth further, a modified parallel-coupled filter structure is introduced. Compared to the traditional parallel-coupled filter, this new structure has better upper stopband performance. The new structure is suitable for broadband active filters with a bandwidth up to 40 percent. All of the active filters described previously are suitable for microwave monolithic integrated circuit (MMIC) due to their planar structures. A one-pole MMIC fixed frequency active filter is designed.

TABLE OF CONTENTS

LIST OF FIGURES

LIST OF TABLES

CHAPTER 1: INTRODUCTION

Active filter is a well known device in low frequency range. The purposes of using an active filter in these frequencies are to increase the element Q value and to reduce the circuit size. In low frequencies, the inductor is bulky and has low Q value. The inductor can be eliminated using an operational amplifier with capacitors and resistors. The operational amplifier transfers the capacitive impedance to the inductive impedance. However, as frequency goes up to microwave frequency, it is impossible to make a device with operational amplifier characteristics, because the active device, namely transistor, has insufficient gain and unpredictable phase change.

Because of the progress in GaAs processing technology, the microwave monolithic integrated circuit (MMIC) has made great advancement. Now, almost all of the microwave circuits from small signal to moderate power can be fabricated using MMIC technology. The MMIC circuits such as low noise amplifiers, power amplifiers, mixers, oscillators, frequency multipliers, etc. have been reported [1]. However, it is still very difficult to make a filter in MMIC form because of the low Q value of MMIC elements. This makes full integration of a microwave system difficult. To overcome this problem, an active filter concept is a hopeful approach.

Previous works in microwave active filter are summarized as following:

In the lower microwave frequencies a method called inverted collector transistor configuration has been reported [2-3]. A lumped inductor is connected to the base of this inverted collector transistor. Looking into the emitter of this transistor, the circuit looks like a inductor in series with a negative resistor. Using this simulated inductor in

parallel with a capacitor, a lossless parallel tank circuit is formed. The active filter made by this active tank circuit shows great performance improvement in the passband region. Because the active device is bipolar transistor, the operating frequency is limited.

Another method uses transversal principle [4-6]. This method is adopted from digital filter concept. The specified frequency response of a filter is Fourier transformed to get the Fourier components. A multi-branched circuit realizes these Fourier components. Each branch has an amplifier or an attenuator to get the correct amplitude and phase for the Fourier component. The filter synthesized in this manner has periodic passband, and usually has very broad bandwidth.

A dielectric active filter circuit based on energy injection concept has been reported [7]. The dielectric resonator is in the shunt feed-back path of a metal-semiconductor field effect transistor (MESFET), therefore the dielectric tank circuit Q is increased significantly. However, the non-planar structure makes it difficult for use in a MMIC circuit.

Based on the same concept as the inverted collector transistor method described previously, an active series tank circuit using a MESFET has been reported [8]. A MESFET connected with inductors and capacitors make the circuit act as a capacitor in series with a negative resistor. An active tank circuit is formed by connecting an inductor in series with this active capacitor. Using this active tank circuit, an active filter is built. In the multi-pole situation, the filter circuit need isolation walls between adjacent tanks. This requirement makes it difficult for use in MMIC circuit.

The objective of this work is to develop an effective way to design a microwave active filter suitable for MMIC applications. The circuit should be planar to meet the requirement of MMIC fabrication. The active device should be a device that has been used in current MMICs. The filter can be designed using commercial available CAD tools. To meet these requirements, a coupled negative resistance method is introduced.

In the second chapter, we describe the theory of a bandpass filter and discuss the basic structure of the coupled negative resistance active tank circuit. The advantage of this type of active tank circuit is discussed. The effect of finite tank circuit unloaded Q on the filter performance is also reviewed. In this chapter we also discuss how to make a negative resistance circuit by a MESFET.

In the third chapter, we describe a narrow band active filter. The fundamental component of this filter is an end-coupled microstrip filter. The design equations of this type of filter is reviewed. Two filter examples are designed and fabricated. In this chapter the details of how to handle the losses in the CAD program is also discussed. An MMIC one-pole active filter with passband center frequency of 17 GHz and 3-dB bandwidth of 70 MHz is designed. In the MMIC design, we use Hughes company's MESFET model and their MMIC fabrication rules. The computer predicted performance is shown. The chip size is about 3 millimeter by 1 millimeter.

The fourth chapter focuses on how to broaden the active filter bandwidth. Due to the fact that coupling between resonators is weak in the end-coupled filter structure, the active filter formed by this structure can only have very narrow bandwidth. In this chapter, we developed a modified end-coupled structure which

can broaden the bandwidth by a factor of 5 to 20. Three filters with different bandwidth are built. The modified end-couple structure make the filter usable up to about 10 percent bandwidth. The design equations are also derived in this chapter.

In the fifth chapter, we introduce a modified parallel-coupled filter structure. The parallel-coupled filter have been used as a popular filter structure for more than 30 years. This type of filters have a bandwidth up to 40 percent. However, since the half-wavelength tanks of this type of filters are not exposed to the outside, it can not be applied to the active filter circuits described in previous chapters. The modified structure is suitable for building an active filter because the tank circuits in the new structure are exposed to the outside. The design procedures of the new filter are developed. Compared to the traditional parallel-coupled filter, the new structure shows better upper stopband performance. Several filters are built to verify the stopband performance improvement. Using this structure an active filter with bandwidth up to 40 percent is possible.

In the sixth chapter, we describe a varactor tuned active filter. A varactor is introduced into the active tank circuit mentioned previously. The varactor makes the tank circuit resonance frequency changes in accordance with the bias voltage. Using this active tank to build the filter makes the filter passband frequency tunable. Two examples are built to verify the validity of tunable active filter. The tuning range is about 500 MHz with 10 GHz center frequency.

Conclusions are given in the seventh chapter, and applications of these circuits are also discussed.

CHAPTER 2: THE BASIC THEORY AND STRUCTURE

In this chapter, we introduce the basic way to synthesize a bandpass filter. The way to synthesize passive bandpass filter described in this chapter will be used in following chapters. The equations are generalized to be used in most kinds of bandpass filters including either lumped element or distributed element filters.

Usually, the design of a bandpass filter starts from a lowpass prototype filter as shown in Fig. 2.1. In Fig. 2.1, the values of g_i's are given by Eqs. 2.1 and 2. 2 [9-10]. Eq. 2.1a through Eq. 2.1h give the g_i value for a lowpass prototype filter having Chebyshev response.

$$\beta = \ln\left(\coth\frac{L_{Ar}}{17.37}\right) \qquad (2.1a)$$

$$\gamma = \sinh\left(\frac{\beta}{2n}\right) \qquad (2.1b)$$

$$a_k = \sin\left[\frac{(2k-1)\pi}{2n}\right], \quad \text{where } k=1,2,\ldots,n \qquad (2.1c)$$

$$b_k = \gamma^2 + \sin^2\left(\frac{k\pi}{n}\right), \quad \text{where } k=1,2,\ldots,n \qquad (2.1d)$$

$$g_0 = 1 \qquad (2.1e)$$

$$g_1 = \frac{2a_1}{\gamma} \qquad (2.1f)$$

$$g_k = \frac{4a_{k-1}a_k}{b_{k-1}g_k}, \quad \text{where } k=2,3,\ldots,n \qquad (2.1g)$$

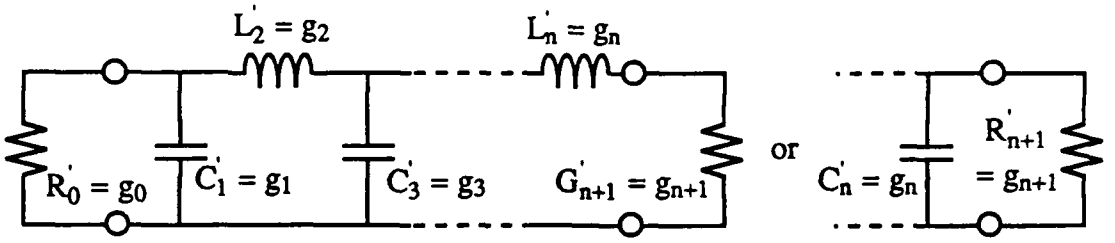

(a)

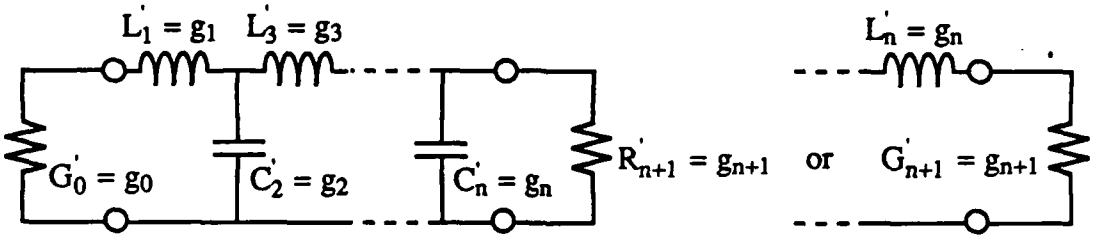

(b)

Fig. 2.1 Definition of lowpass prototype filter parameters.

$$g_{n+1} = 1 \ , \qquad \text{for n odd}$$

$$= \coth^2 \left(\frac{\beta}{4}\right) , \qquad \text{for n even} \qquad (2.1h)$$

where the term L_{Ar} is defined as passband ripple for a Chebyshev filter. Eq. 2.2a through Eq. 2.2c give the value of g_i for a lowpass prototype filter having maximally flat response.

$$g_0 = 1 \qquad (2.2a)$$

$$g_k = 2 \sin \left[\frac{(2k-1)\pi}{2n}\right] , \qquad \text{where } k=1,2,...,n \qquad (2.2b)$$

$$g_{n+1} = 1 \qquad (2.2c)$$

The prototype filter has normalized characteristics which shows a cutoff angular frequency 1 rad/sec. and source resistance 1 Ω. The cutoff frequency means the frequency where the filter response shows specific loss and begins to roll off. The specific loss value for a Chebyshev filter is L_{Ar} (passband ripple) and for a maximally flat filter is 3 dB.

Fig.2.2 shows the lowpass to bandpass transformation. The filter frequency response is also transformed as shown in Fig. 2.3. For any kind of series resonator the reactance slope parameter is defined as :

$$x = \frac{\omega_0}{2} \frac{dX}{d\omega}\Bigg|_{\omega_0} \qquad \text{ohms} \qquad (2.3a)$$

For any kind of parallel resonator the susceptance slope parameter is defined as :

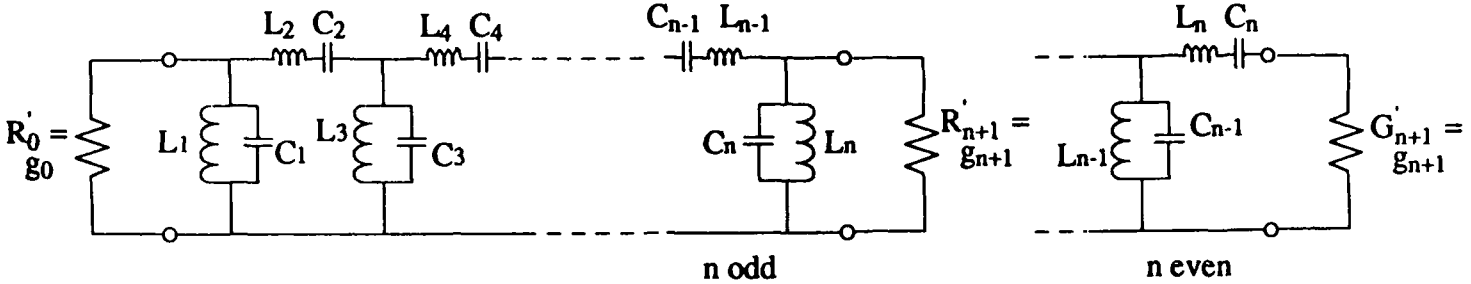

(a) The bandpass filter transformed from Fig. 2.1a.

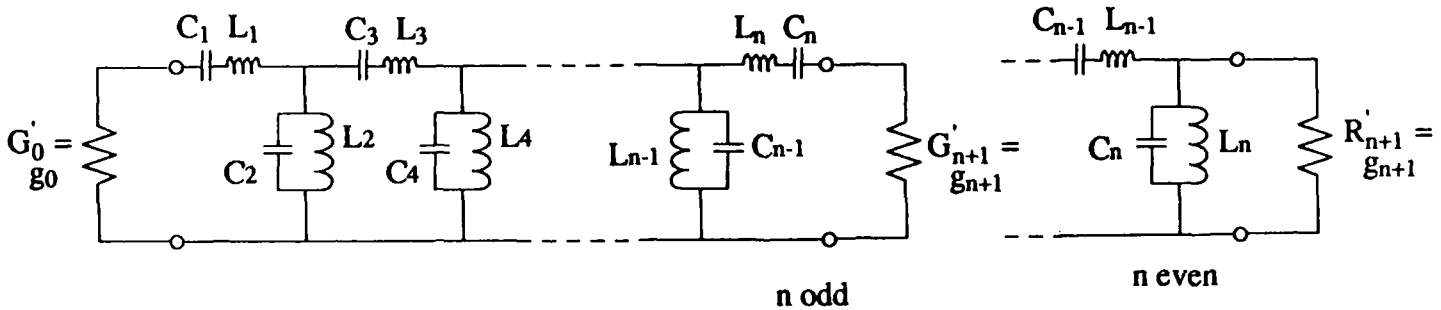

(b) The bandpass filter transformed from Fig. 2.1b.

Fig. 2.2 The lowpass to bandpass transformation.

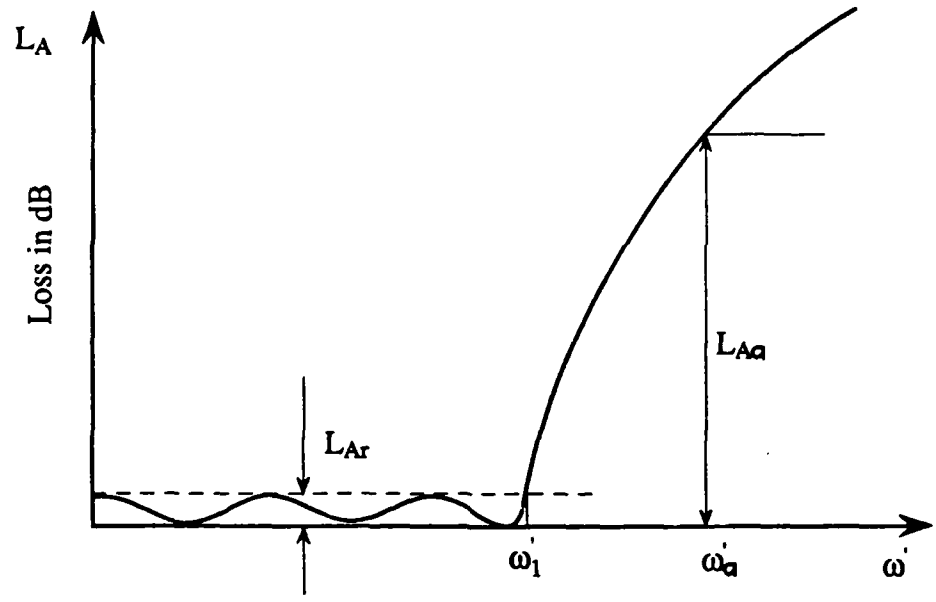

(a) The prototype lowpass filter frequency response.

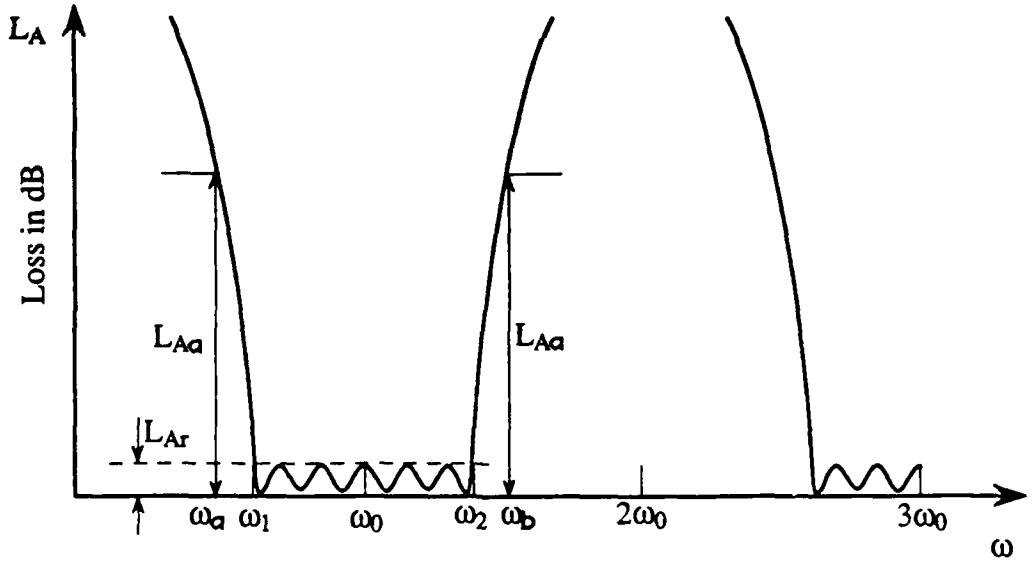

(b) The frequency response of bandpass filter transformed from lowpass prototype filter.

Fig. 2.3 Lowpass prototype response and corresponding bandpass filter response.

$$b = \frac{\omega_0}{2}\frac{dB}{d\omega}\Big|_{\omega_0} \quad \text{siemens} \qquad (2.3b)$$

where the ω_0 is the resonant frequency of the resonator.

The susceptance and impedance slope parameters in Fig. 2.2 are given as follows :

For shunt resonators :

$$b_j = \omega_0 C_j = \frac{1}{\omega_0 L_j} = \frac{\omega_1' g_j}{w} = \text{susceptance slope paramerter} \qquad (2.4a)$$

For series resonators :

$$x_k = \omega_0 L_k = \frac{1}{\omega_0 C_k} = \frac{\omega_1' g_k}{w} = \text{reactance slope paramerter} \qquad (2.4b)$$

where ω_1' is the transformed normalized cutoff angular frequency, namely, 1 rad/sec., and w is relative bandwidth of bandpass filter which is defined as :

$$w = \frac{\omega_1 - \omega_2}{\omega_0} \qquad (2.4c)$$

and ω_0 in this case is defined as :

$$\omega_0 = \sqrt{\omega_1 \omega_2} \qquad (2.4d)$$

Further transformation is made as shown in Fig. 2.4. The $J_{i,j}$'s and $K_{i,j}$'s are admittance inverters and impedance inverters. Using these inverters the filter can be realized by series resonators or by parallel resonators only.

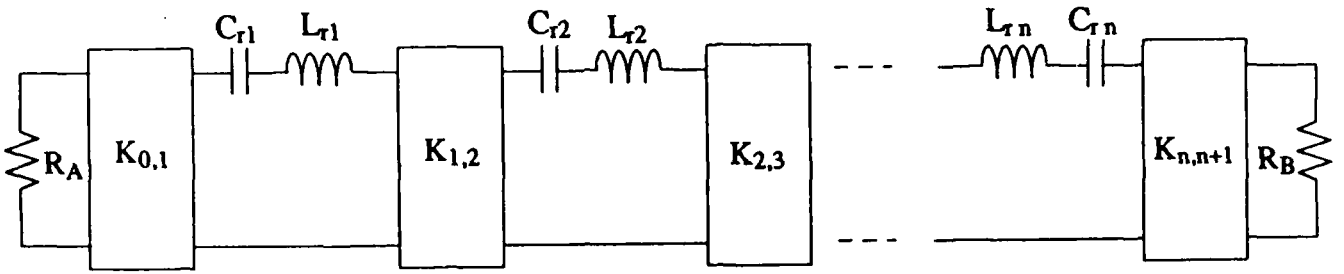

(a) The bandpass filter in Fig.2.2a converted to use only series resonators and impedance inverters.

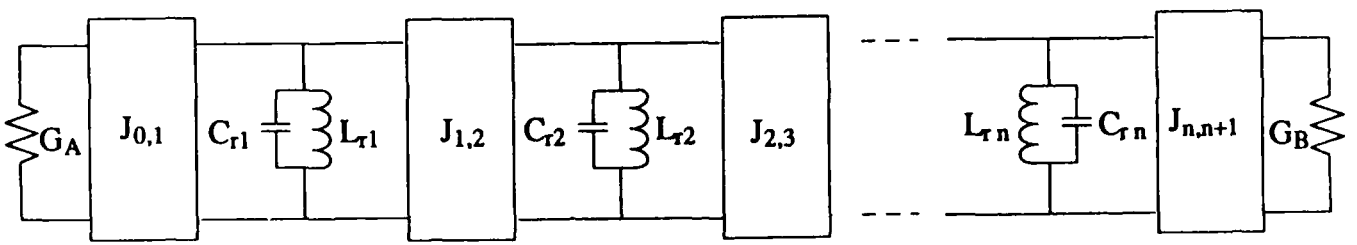

(b) The bandpass filter in Fig.2.2b converted to use only shunt resonators and admittance inverters.

Fig. 2.4 Bandpass filter converted from Fig. 2.2 using only series or shunt resonators.

A more generalized configuration of a bandpass filter is shown in Fig.2.5. The filter consists of coupling structures and tank circuits. The tank circuit in this report means a resonant structure. In the lumped circuit case it is either a series or a parallel LC (L is an inductor, and C is a capacitor) circuit. In the distributed circuit case it is either a half wavelength or a quarter wavelength transmission line. The distributed tank circuit can be equivalent to a LC tank circuit [11]. The coupling structures function as impedance or admittance transformers. Usually, these transformers are called J (for admittance transformer) or K (for impedance transformer) inverters as mentioned previously. In Fig. 2.5, the J and K values are given by Eqs. 2.5 and Eqs. 2.6.

For the filter shown in Fig. 2.5a :

$$b_j = \frac{\omega_0}{2}\frac{dB_j}{d\omega}\Big|_{\omega_0} \quad \text{siemens} \qquad (2.5a)$$

$$J_{0,1} = \sqrt{\frac{G_A b_1 w}{g_0 g_1 \omega_1}} \qquad (2.5b)$$

$$J_{j,j+1} = \frac{w}{\omega_1}\sqrt{\frac{b_j b_{j+1}}{g_j g_{j+1}}} \quad , \text{where } j = 1,2,\ldots,n-1 \qquad (2.5c)$$

$$J_{n,n+1} = \sqrt{\frac{G_B b_n w}{g_n g_{n+1} \omega_1}} \qquad (2.5d)$$

For the filter shown in Fig. 2.5b :

$$x_j = \frac{\omega_0}{2}\frac{dX_j}{d\omega}\Big|_{\omega_0} \quad \text{ohms} \qquad (2.6a)$$

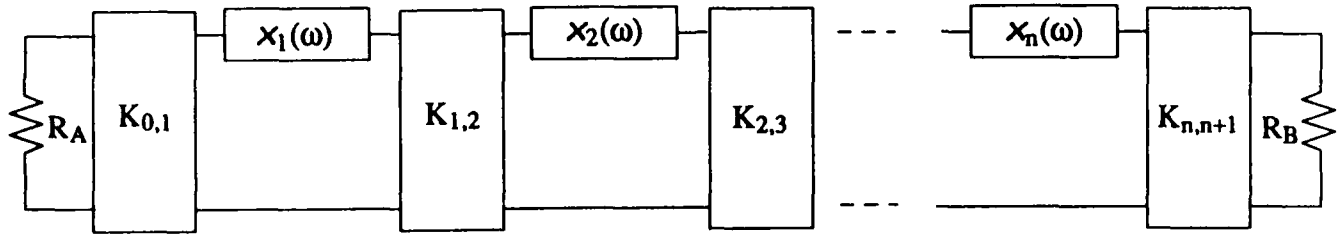

(a) Generalized bandpass filter developed from Fig. 2.4a.

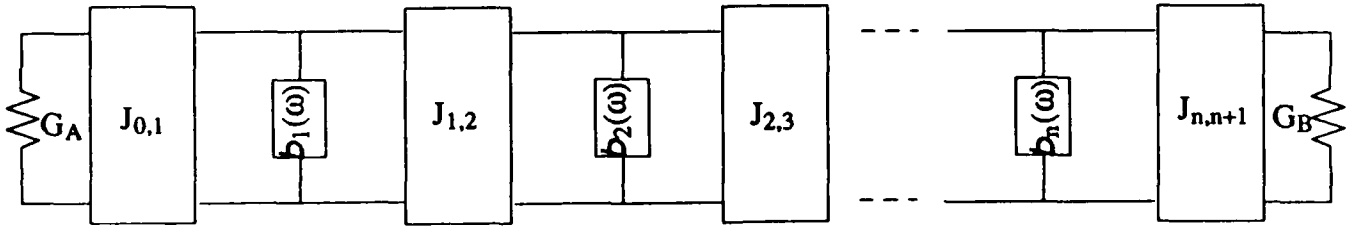

(b) Generalized bandpass filter developed from Fig. 2.4b.

Fig. 2.5 Generalized bandpass filter using J or K inverters and generalized tanks.

$$K_{0,1} = \sqrt{\frac{R_A X_1 w}{g_0 g_1 \omega_1'}} \qquad (2.6b)$$

$$K_{j,j+1} = \frac{w}{\omega_1'}\sqrt{\frac{X_j X_{j+1}}{g_j g_{j+1}}} \quad , \text{where } j = 1,2,...,n-1 \qquad (2.6c)$$

$$K_{n,n+1} = \sqrt{\frac{R_B X_n w}{g_n g_{n+1} \omega_1'}} \qquad (2.6d)$$

In order for the planar circuit structure to meet the MMIC requirement, we concentrate on the microstrip filters throughout this report. In most of the microstrip filter, the tank circuit is formed by an open circuit half wavelength transmission line, therefore, the tank circuit is equivalent to a parallel LC circuit [11], and the J-inverter is used to couple each tank circuit. Therefore, the equivalent circuit of a microstrip bandpass filter can be equivalent to Fig. 2.5b or, more precisely, Fig. 2.4b. The susceptance slope parameter of an open circuit half wavelength transmission line tank circuit is given by:

$$b_j = \frac{\pi}{2} Y_0 \qquad (2.7)$$

where Y_0 is the characteristic admittance of the transmission line. Substituting Eq. 2.7 into Eqs. 2.6 and with the $g_{i,j}$ values obtained from Eqs. 2.1 (or Eqs. 2.2, depend on the filter response) the $J_{i,i+1}$ values can be obtained.

Bandpass filters synthesized as described above are called coupled-resonator filters. Filters of this type can have ideal Chebyshev or maximally flat responses only when the tank circuit is lossless. The effect of the lossy tank on the filter response

have been reported [12]. Fig. 2.6 are computer simulated filter responses with lossy tank. The figures show how the finite tank circuit unloaded Q value degrades the filter response. The effects of tank circuit loss on the filter performance are summarized as follows :

(1). The passband insertion loss and V.S.W.R. increases.

(2). In the multi-pole case (as in Fig. 2.6b), two passband corners are rounded. Here, we call it passband corner rounding effect.

(3). It has very small influence on the stopband performance.

For simplicity, we use a one-pole lumped element filter structure to explain the effect of the finite tank circuit Q on the filter performance. Fig. 2.7 shows the one-pole filter with a lossy tank. In Fig. 2.7, if R = 0, the filter is called lossless filter. The 1/w value in Eq. 2.4c of a lossless one-pole filter called Q_{design} which depends on the R_S, R_L, L, C,and J values in Fig. 2.7. Therefore, Q_{design} can be obtained by measuring the 3-dB points and the center frequency of the lossless circuit. However, if the tank is lossy, in other words $R \neq 0$, the circuit measured Q value will degrade from Q_{design} to Q_{eff}. Eqs. 2.8 describe the relations between tank circuit unloaded Q (Q_{tank}), the effective circuit Q with a lossy tank (Q_{eff}), and the designed circuit Q based on lossless tank (Q_{design}).

$$\frac{1}{Q_{eff}} = \frac{1}{Q_{design}} + \frac{1}{Q_{tank}} \qquad (2.8a)$$

where the tank circuit unloaded Q (Q_{tank}) is defined as [11] :

$$Q_{tank} = \frac{\omega_0 L}{R} \qquad (2.8b)$$

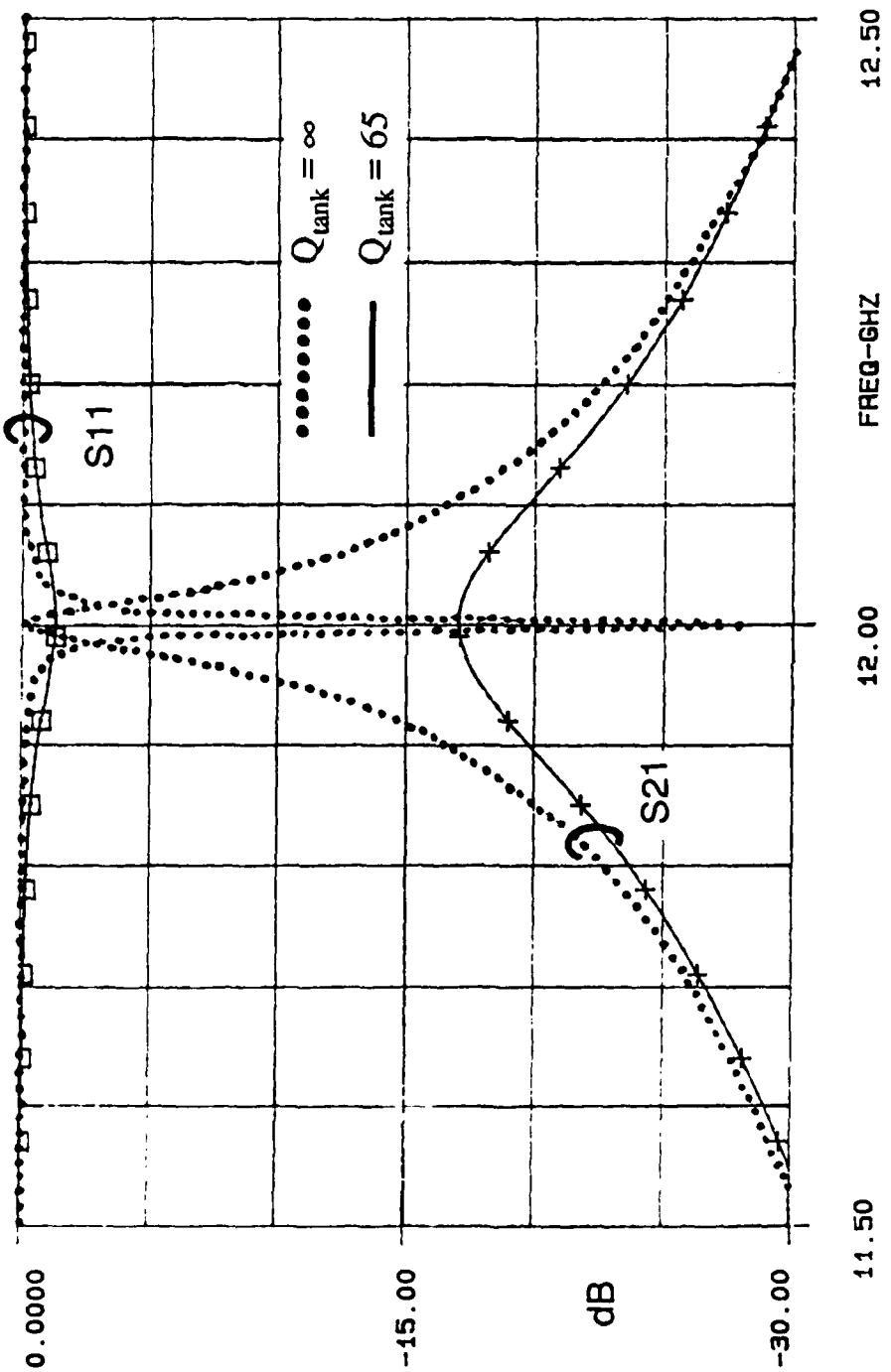

Fig. 2.6a The effect of finite tank circuit Q on 1-pole filter performance.
The designed circuit Q (Q_{design}) = 400.

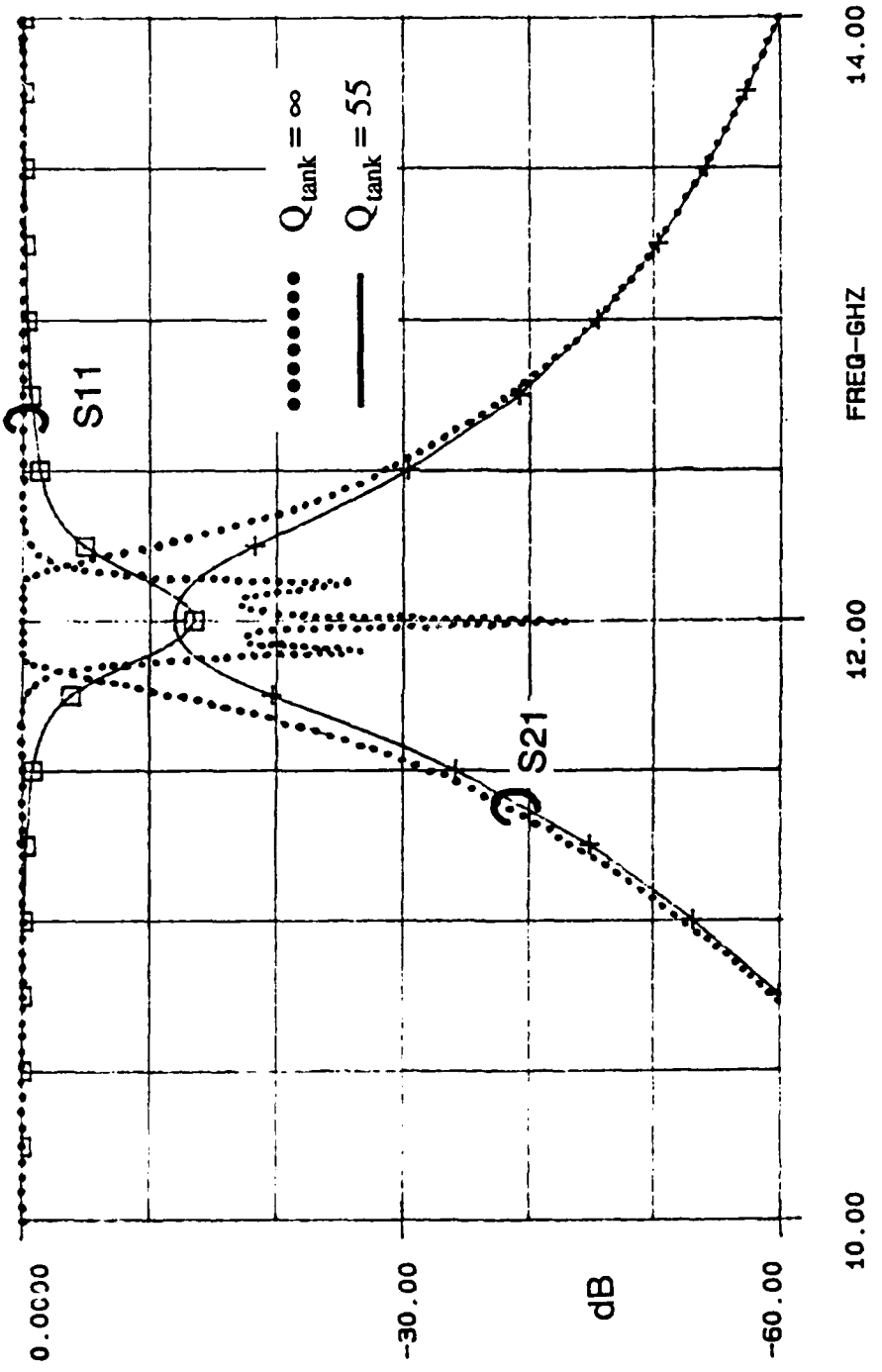

Fig. 2.6b The effect of finite tank circuit Q on 3-pole filter performance.
The filter is designed to have 3% bandwidth at 12 GHz with .1 dB ripple.

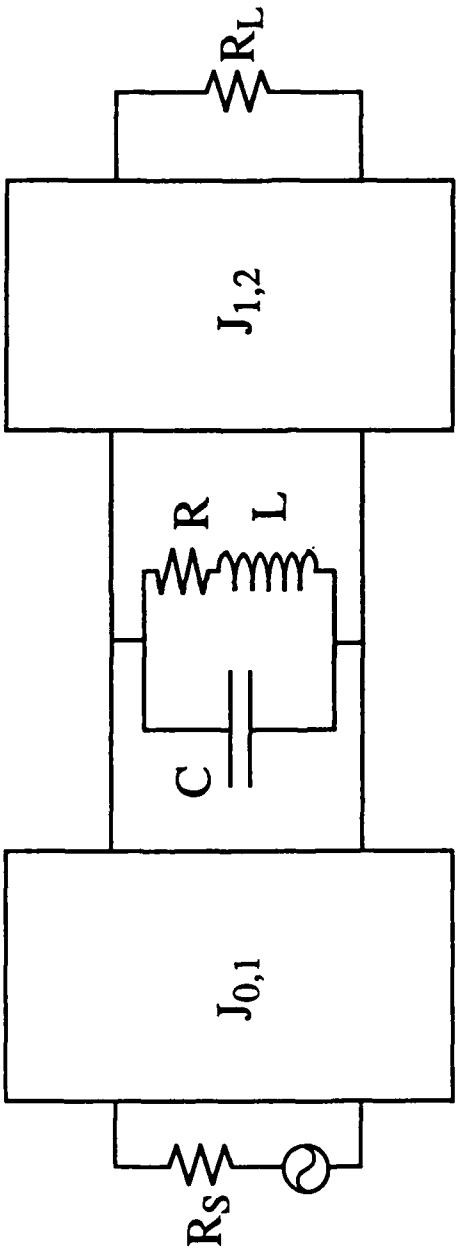

Fig. 2.7 One-pole bandpass filter with lossy tank and J-inverters.

From Eqs. 2.8, if the tank is lossless, then $Q_{tank} = \infty$ and $Q_{eff} = Q_{design}$, and if the tank is lossy, then Q_{eff} can never be higher than Q_{tank}. This means that we can never make a filter with the circuit Q value higher than tank circuit unloaded Q value. From previous explanation it is apparent that the key point to make a good bandpass filter is to increase the tank circuit Q value. This is why most of the reported work on microwave active filters concentrate on how to increase the tank circuit Q value [2,3,7,8].

Here, we introduce a method called the coupled negative resistance method to increase the tank circuit Q value. Fig. 2.8a and Fig. 2.8b show the generalized equivalent circuit of a coupled negative resistance structure. A lossy tank circuit consisting of L, C, and R_p is coupled to a negative resistance circuit R_n as shown in Fig. 2.8a and Fig. 2.8b. If we properly adjust the coupling value, R_p and R_n values the dissipating resistor R_p can be canceled out by the coupled negative resistance R_n. In Fig. 2.8a and Fig. 2.8b, the negative resistance circuit is a generalized representation of any kind of circuit which can make the impedance have a negative real part. In this report, MESFETs are used to realize the negative resistance circuit. Fig. 2.8c show the concept of the coupled negative resistance method realized in a possible microstrip circuit form. Fig. 2.8b is also the equivalent circuit of Fig. 2.8c. The advantage of this type of active tank over other types of approach summarizes as follows:

(1). Compared to the lumped element active tank realized by directly cancelling the dissipating resistance [2,3,8], the coupled negative resistance method is less influential to the variation of passive and active devices parameters. For

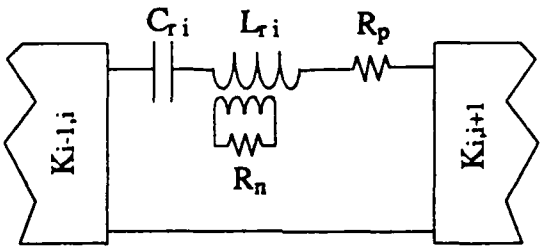

(a) Series active tank.

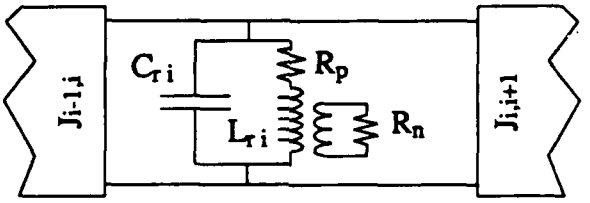

(b) Shunt active tank.

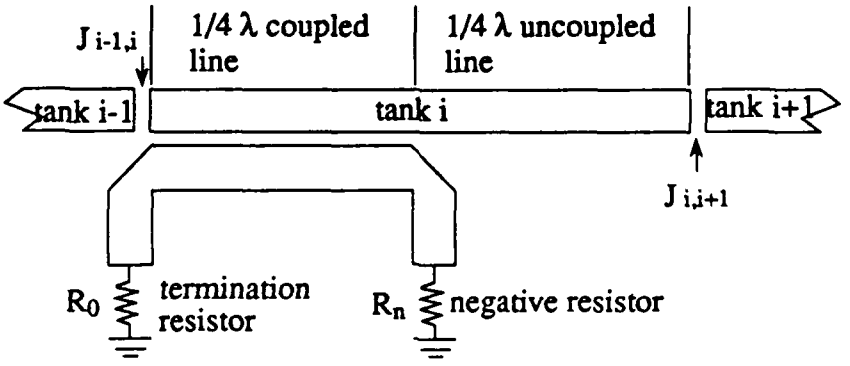

(c) The microstrip active tank circuit.

Fig. 2.8 The active tank based on coupled negative resistance method.

example, to make a microstrip half wavelength resonator at X-band the line length tolerance can be controlled to within 0.1 percent. However, the tolerance of a lumped capacitor is about 1 percent. Another important thing is that the active device placed inside the tank circuit make the tank characteristics to vary easily as the active device parameters changed.

(2). Compared to digital filter approach [4-6], the coupled negative resistance method can be used in a very narrow bandwidth (much less than 1 percent bandwidth) case.

(3). As opposed to the method of placing the tank circuit in the FET's shunt feedback path [7], the coupled negative resistance method uses a planar structure. This is a basic criterion of MMIC fabrication. Another advantage is that this method uses the easier design procedures than the procedures in [7].

The coupled negative resistance active tank circuit in microstrip line form consist of a half wavelength microstrip tank, a quarter wavelength coupler, and a negative resistance circuit as shown in Fig. 2.8c. We describe a MESFET negative resistance circuit which will be used in the following four chapters.

For solid state devices like tunnel, Gunn, and IMPATT diodes, when it is biased with the proper D.C. voltage or current the device will produce a negative resistance at the device terminals. For these two-terminal devices, the negative resistance can extend up to millimeter (30 to 300 GHz) or sub-millimeter (300 to 3000 GHz) wave frequency range. However, accurate negative resistance circuit models for two terminal devices are difficult to obtain. Here, we choose three-

terminal devices, namely the MESFET, to produce negative resistance. Throughout this report the active devices used to produce negative resistance are NEC-71083 70mil ceramic-packaged MESFETs. The MESFETs can produce negative resistance by proper feedback. There are two kinds of feedback, namely series and shunt feedback, which produce negative resistance. Fig. 2.9 shows the feedback configurations [13]. The series feedback was chosen, for its elements are simply connected. Fig.2.10 shows two examples of the negative resistance circuit. The basic configuration in Fig. 2.10 is series feedback with grounded gate. The source inductor enhances the negative resistance value. In Fig. 2.10a the gate feedback element is a lowpass filter, which is designed with 82 ohm system impedance, 7-pole, maximally flat response, and 8.2 GHz cutoff frequency. The lowpass filter is realized with quasi-lumped circuit approach. The inductors are realized by microstrip high impedance lines, and the capacitors are realized by low impedance lines. The step discontinuities between high impedance and low impedance lines are taken into account. The computer simulated performances of circuit in Fig. 2.10a are shown in Fig. 2.11a. This circuit produces negative resistance from 9 GHz to 18 GHz. In Fig 2.10b, the gate feedback lowpass filter is changed to an inductor with one end grounded. The inductors in Fig. 2.10 are realized by high impedance microstrip lines. Computer calculated results of the circuit in Fig. 2.10b are shown in Fig. 2.11b. The negative resistance circuit of this type produces negatives resistance from 4.5 to 20 GHz.

In this chapter we have attempted to provide insight into the operation of the coupled-resonator bandpass filter. The effect of tank circuit loss on the bandpass filter performance have been discussed. The coupled negative resistance method to

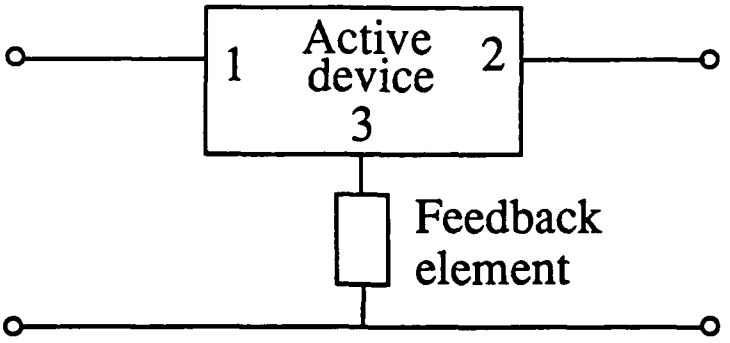

(a) Series feedback configuration.

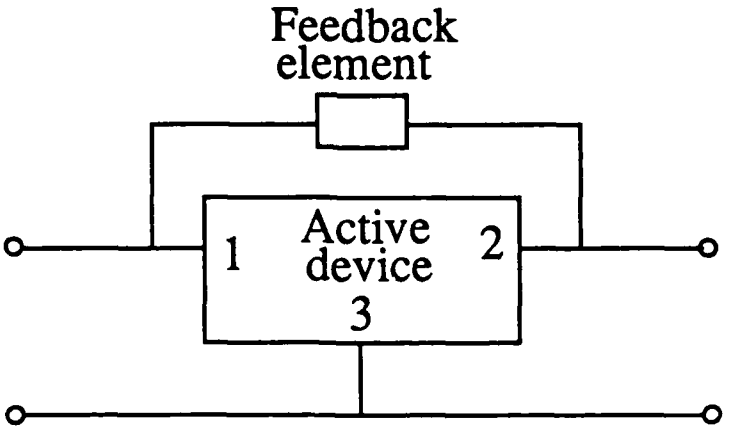

(b) Shunt feedback configuration.

Fig. 2.9 Two types of feedback configuration.

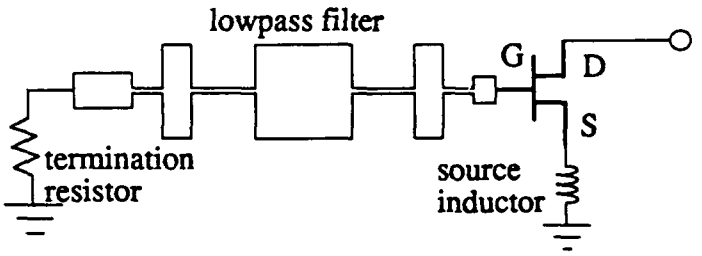

(a) Negative resistance circuit with gate feedback lowpass filter.

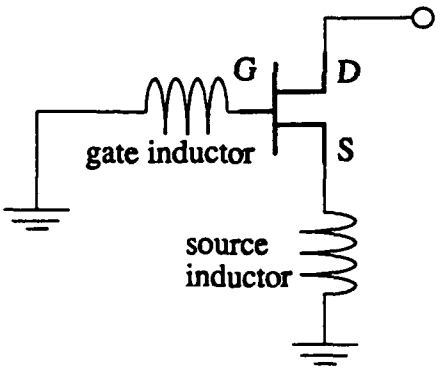

(b) Negative resistance circuit with gate feed back inductor.

Fig. 2.10 The basic structures of negative resistance circuit.

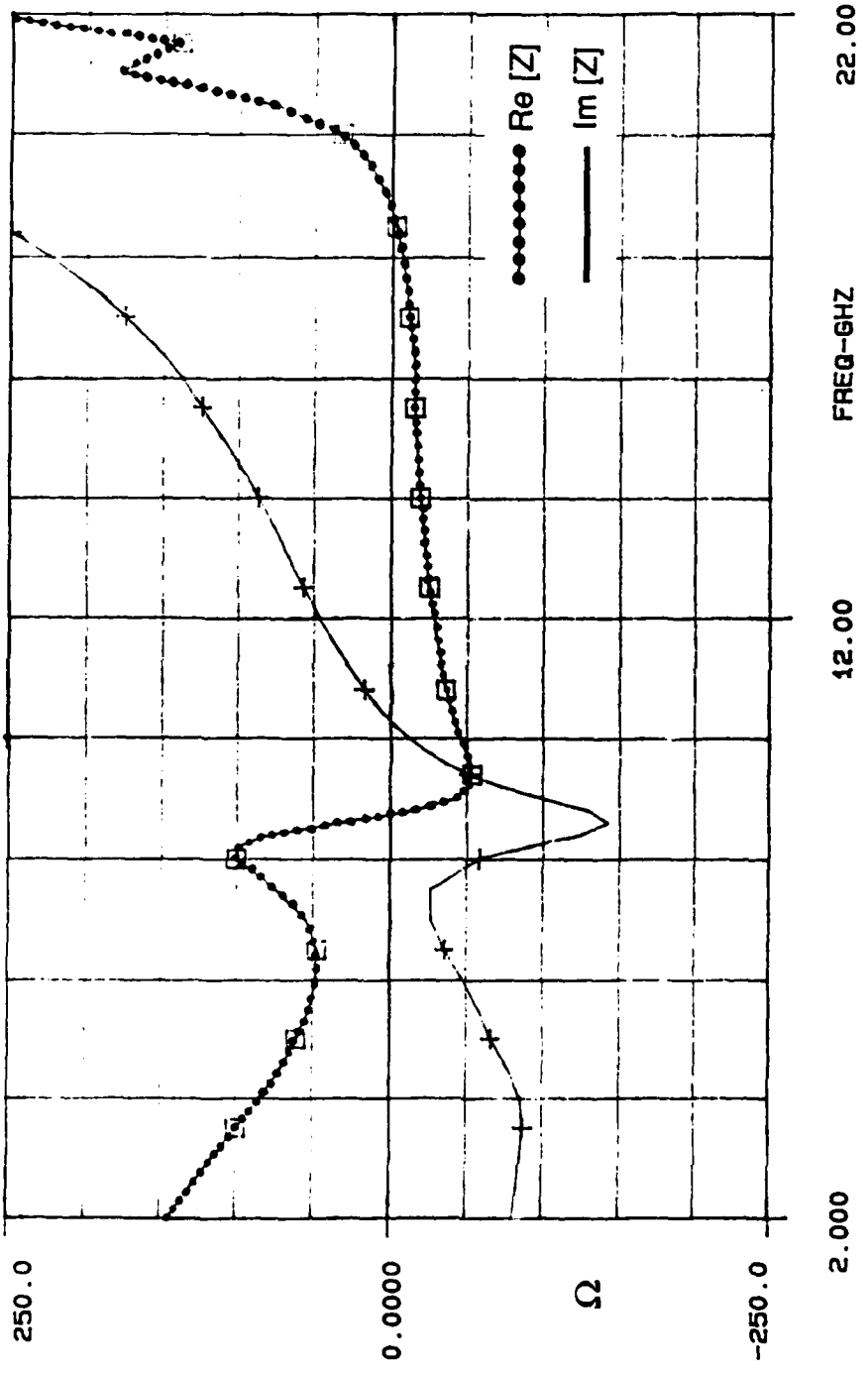

Fig. 2.11a The simulated performance of the negative resistance circuit as shown in Fig. 2.10a.

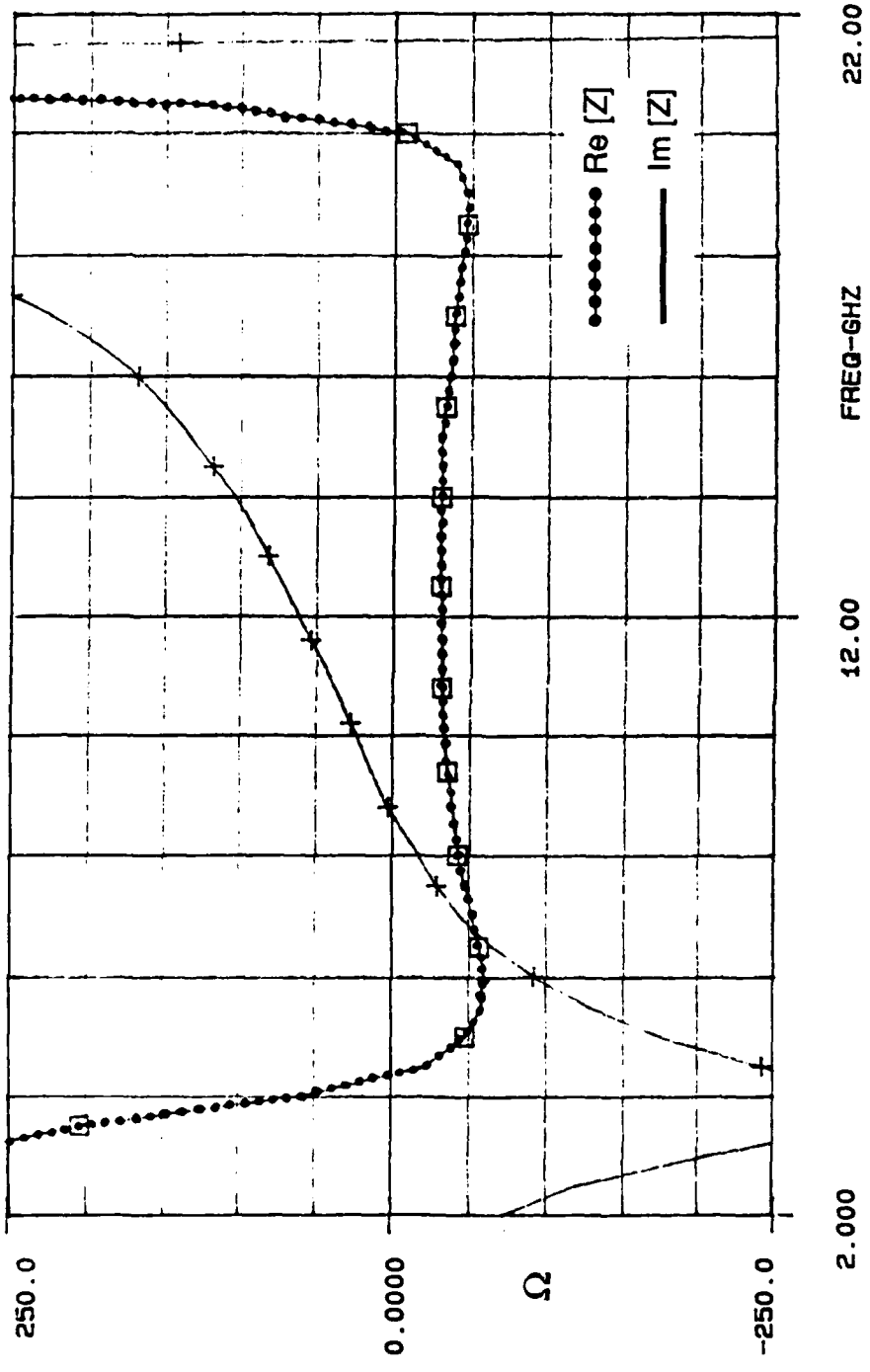

Fig. 2.11b The simulated performance of the negative resistance circuit as shown in Fig. 2.10b.

make an active tank circuit has been presented and the advantages of this method over other methods have also been discussed. Finally, we provide a MESFET negative resistance circuit which will be used in the circuit of following chapters.

CHAPTER 3: NARROW BAND ACTIVE FILTERS

In the previous chapter, we introduced the basic theory of operation of the coupled negative resistance method. An end-coupled active filter based on the active microstrip tank shown in Fig. 2.8c is shown in Fig. 3.1 [14-15]. This filter uses the simplest coupling structure, namely the microstrip gap, to form J-inverters. In order to synthesize the filter closed form equations for equivalent circuit model of the microstrip gaps are obtained. Here, the microstrip gap equivalent circuit model developed by Silvester and Benedek [16] and curvefitted by Hammerstad [17] were chosen. The microstrip gap equivalent circuit is shown in Fig. 3.2. The values of the circuit parameters are given by Eqs. 3.1

$$u = \frac{w_{strip}}{h} \tag{3.1a}$$

where w_{strip} is the microstrip line width, and h is the substrate thickness.

$$\frac{\Delta_e}{h} = 0.102 \frac{u + 0.106}{u + 0.264} \{ 1.166 + \frac{\varepsilon_r + 1}{\varepsilon_r} [0.9 + \ln (u + 2.475)] \} \tag{3.1b}$$

where ε_r is the relative dielectric constant of the substrate, and Δ_e is the microstrip open end equivalent length.

$$\frac{B_{j,j+1} \lambda_g}{Y_0 h} = 2.4 \frac{u + 0.1}{u + 1} \sqrt{\frac{\varepsilon_r + 2}{\varepsilon_r + 1}} \ln (\coth (\frac{\varepsilon_r s_{j,j+1}}{(\varepsilon_r + 2) h})) \tag{3.1c}$$

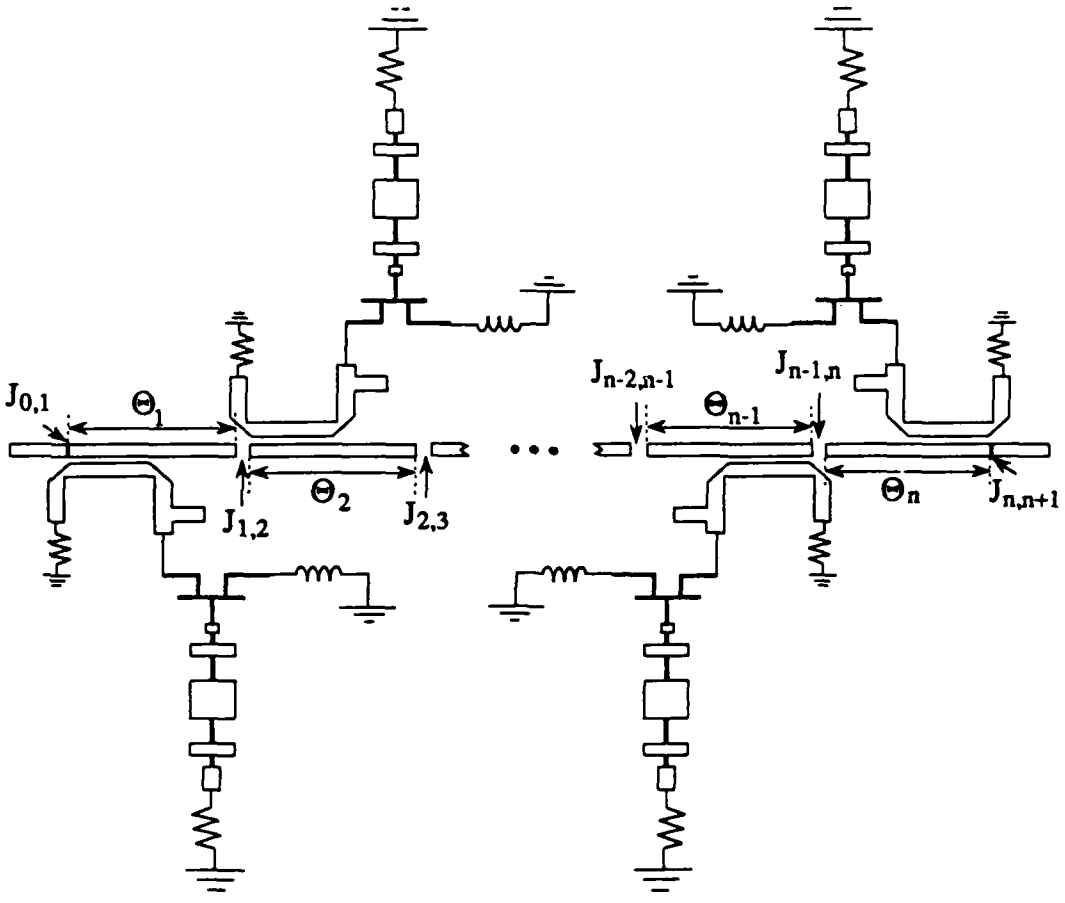

Fig. 3.1 The circuit configuration of end-coupled active filter.

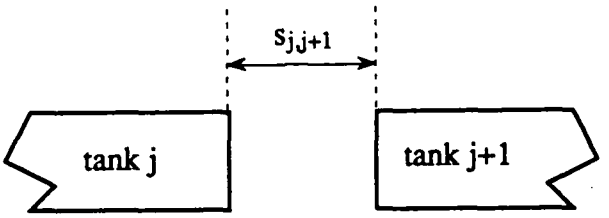

(a). The microstrip gap with gap width equals $s_{j,j+1}$.

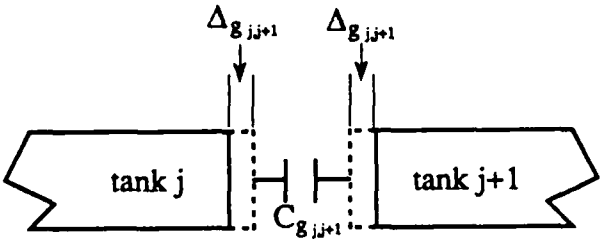

where $\omega C_{g\,j,j+1} = B_{j,j+1}$

(b). The equivalent circuit of (a).

Fig. 3.2 The equivalent circuit of a microstrip gap.

where $B_{j,j+1}$ is the susceptance value of the gap capacitor between the j'th and j+1'th tank; Y_0 is the characteristic admittance of the tank microstrip line; λ_g is the guided wavelength of wave traveling in the microstrip line, and $s_{j,j+1}$ is the gap width between j'th and j+1'th tank.

$$\frac{\Delta_{p\,j,j+1}}{h} = \frac{\Delta_e}{h} \tanh^2 \sqrt{\frac{s_{j,j+1}}{2\,\Delta_e}} \tag{3.1d}$$

and

$$\frac{\Delta_{g\,j,j+1}}{h} = \frac{\Delta_{p\,j,j+1}}{h} + \frac{B_{j,j+1}\,\lambda_g}{2\pi\,Y_0\,h} \tag{3.1e}$$

where j = 0, 1, 2, ..., n, and $\Delta_{g\,j,j+1}$ is the microstrip gap equivalent length extension as shown in Fig. 3.2. $\Delta_{g\,j,j+1}$ in Fig.3.2 is absorbed by each side of the tank circuit when synthesizing the filter. Using the J values obtained in previous chapter, we can obtain the $B_{j,j+1}$ values from Eq. 3.2 [9]:

$$\frac{B_{j,j+1}}{Y_0} = \frac{\frac{J_{j,j+1}}{Y_0}}{1 - (\frac{J_{j,j+1}}{Y_0})^2} \tag{3.2}$$

where j = 0, 1, 2,..., n. From Eqs. 3.1, Eq. 3.2 and the J values obtained from Chapter 2 the gap width between adjacent tanks are obtained.

The electrical length of each tank as shown in Fig. 3.1 is given by Eq. 3.3 [9]. In Eq. 3.3, the equivalent length extensions for gaps, namely $\Delta_{g\,j-1,j}$ and $\Delta_{g\,j,j+1}$, are taken into account.

$$\theta_j = \pi - \frac{1}{2}\left[\tan^{-1}\left(\frac{B_{j-1,j}}{Y_0}\right) + \tan^{-1}\left(\frac{B_{j,j+1}}{Y_0}\right)\right] - 2\pi\left(\frac{\Delta_{g\,j-1,j} + \Delta_{g\,j,j+1}}{\lambda_g}\right) \qquad (3.3)$$

where j = 1, 2, 3,..., n. The filter synthesis procedures are completed from Eqs. 3.1 through Eq. 3.3.

The next step is to insert the active circuit part into the filter. There is one important thing that we should first find out a method which can make Touchstone™ simulator (a product name of EEsof company) take into account the accurate tank circuit loss. The end-coupled filter discussed in this chapter is narrowband because of the weak gap coupling. The loss of a narrowband filter constructed by half wavelength open circuit tanks is mainly from radiation loss of the tanks. However, the Touchstone™ circuit simulator can not take the radiation loss into account. An accurate value of the loss compensation when designing an active filter is very important. Here, we use an experimental method to make a loose coupled tank and measure the unloaded Q value of the tank. The simulated result can be matched to this measured data by increasing the dielectric or conductor loss value at the tank part of the circuit. Using this semi-experimental data to simulate the active filter circuit a good result can be achieved. The measured unloaded Q value at 10 GHz of a half wavelength resonator built on a 30-mil thick one-ounce copper clad woven PTFE substrate is 85. Adjusting the substrate dielectric loss tangent to 0.028 the simulated

result matches the measured result. Using this loss tangent value in the Touchstone™ simulator to optimize the active filter performance, the measured and simulated performance is in good agreement. The substrate introduced here will be used throughout this report.

Based on the filter synthesizing and optimizing procedures outlined above, two example active filters were built. The filter design parameters are listed in Table 3.1. To verify the performance improvement, two corresponding passive filter were also built. The passive filter are designed with same filter parameters and fabricated on the same kind of substrate. Fig. 3.3 shows the measured performance of the one-pole filter. The measured circuit Q value (Q_{eff}) is 250 which is same as the designed circuit Q value (Q_{design}). According to Eq. 2.8a, the tank circuit unloaded Q value (Q_{tank}) is infinity, in other words, the tank circuit is lossless. The measured circuit Q value (Q_{eff}) of the passive filter is 64. From Eq. 2.8a, the tank circuit unloaded Q value (Q_{tank}) is 85. Comparing the active filter and passive filter performance curves in Fig. 3.3, following conclusions can be reached:

(1) The tank circuit unloaded Q (Q_{tank}) has been improved from 85 to infinity.

(2) The active circuit has improved only the performance of the passband region, and the stopband performance was dictated by the original passive circuit.

(3) The passband insertion loss has been improved from 12 dB in the passive filter to 2.5 dB in the active filter.

(4) S_{11} has been improved from -3.5 dB in the passive filter to -30 dB in the active filter at center frequency.

filter type / spec.	1-pole filter	2-pole filter
center frequency	10 GHz	10.4 GHz
3-dB bandwidth	0.4 %	1.73 %
response	max. flat	Chebyshev
ripple	--	0.1 dB
substrate thickness	30 mil	30 mil
substrate dielec. const.	2.55	2.55
system * impedance	82 Ω	82 Ω
1-dB comp. point	-13 dBm at input	--

* : Non-50 Ω system impedance is tapered to 50 Ω at input and output.

Table. 3.1 The filter parameters of fixed frequency end-coupled active filter.

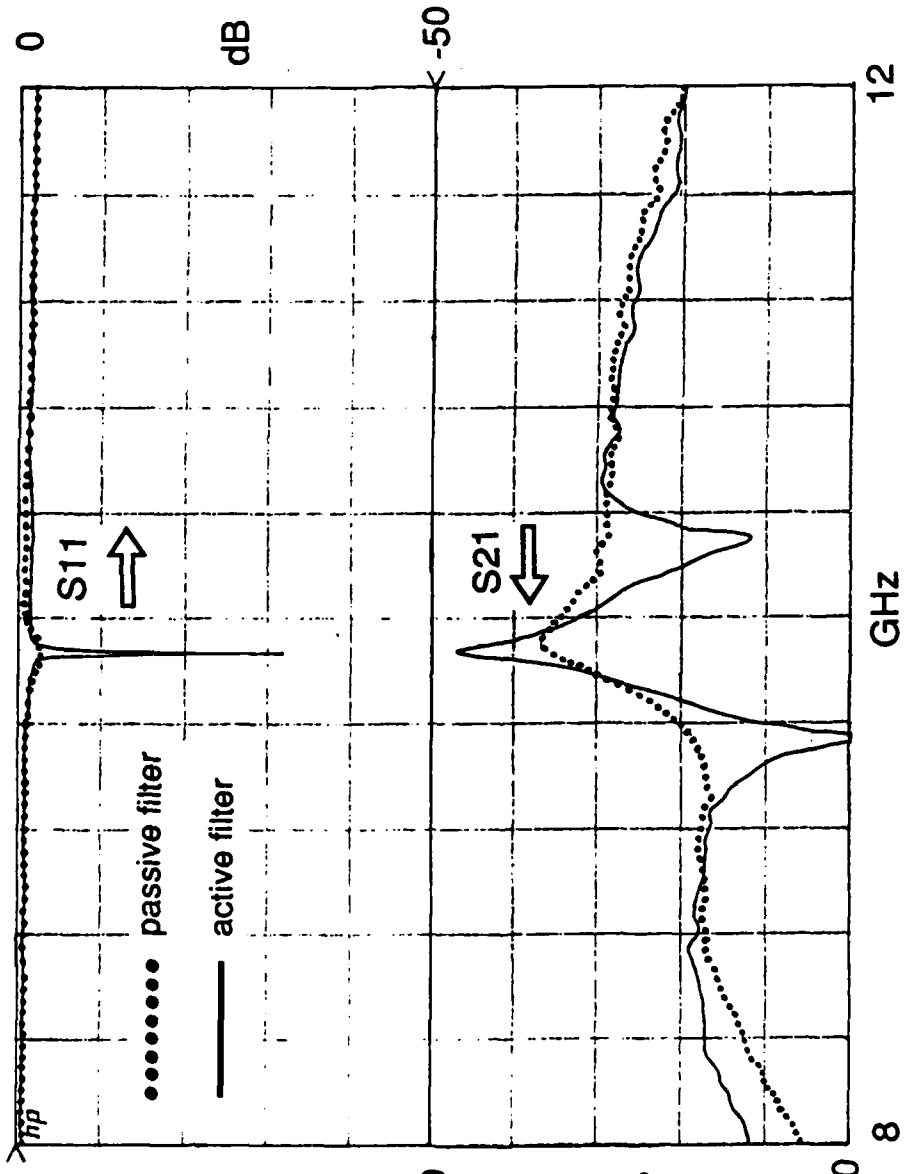

Fig. 3.3 The measured one-pole filter performances.

The one-pole filter is the simplest case. It directly reveals the tank circuit loss condition discussed in Chapter 2. Based on the performance curves for the one-pole filter, the coupled negative resistance method improved the tank circuit unloaded Q value. One important parameter to evaluate the dynamic range of the active filter is the 1-dB compression point. Fig. 3.4 shows the measured 1-dB compression curve of the one-pole active filter. The 1-dB compression point is -13 dBm measured at input.

The 2-pole active and passive filter performance are shown in Fig. 3.5. In this figure, the passband S_{11} and S_{21} performance is improved significantly. S_{21} improves from -9 dB to about 0 dB, and two dips in S_{11} are apparent. Fig. 3.6 shows the computer simulated results of the 2-pole active filter. Fig. 3.7 shows the photograph of the one-pole and 2-pole filters. The DC bias circuit of the MESFETs are shown in Fig. 3.8 This bias is one of the self-bias configurations; in other words, it uses only single power supply to provide both gate and drain bias.

Using the same design procedures described above, a MMIC active filter was designed. In the MMIC, a Hughes Co. developed MESFET is used as active device. The equivalent circuit model provided by Hughes Co. is shown in Fig. 3.9, and the FET parameters are shown in Table 3.2. The negative resistance circuit configuration is the same as in Fig. 2.10b. The simulated negative resistance circuit performance is shown in Fig. 3.10. The chip size of the active filter is limited to an area of 3 millimeter $\times$ 1 millimeter. The substrate used here is 100 microns thick semi-insulating GaAs substrate with dielectric constant of 12.9. Some important fabricating parameters are summarized as follows:

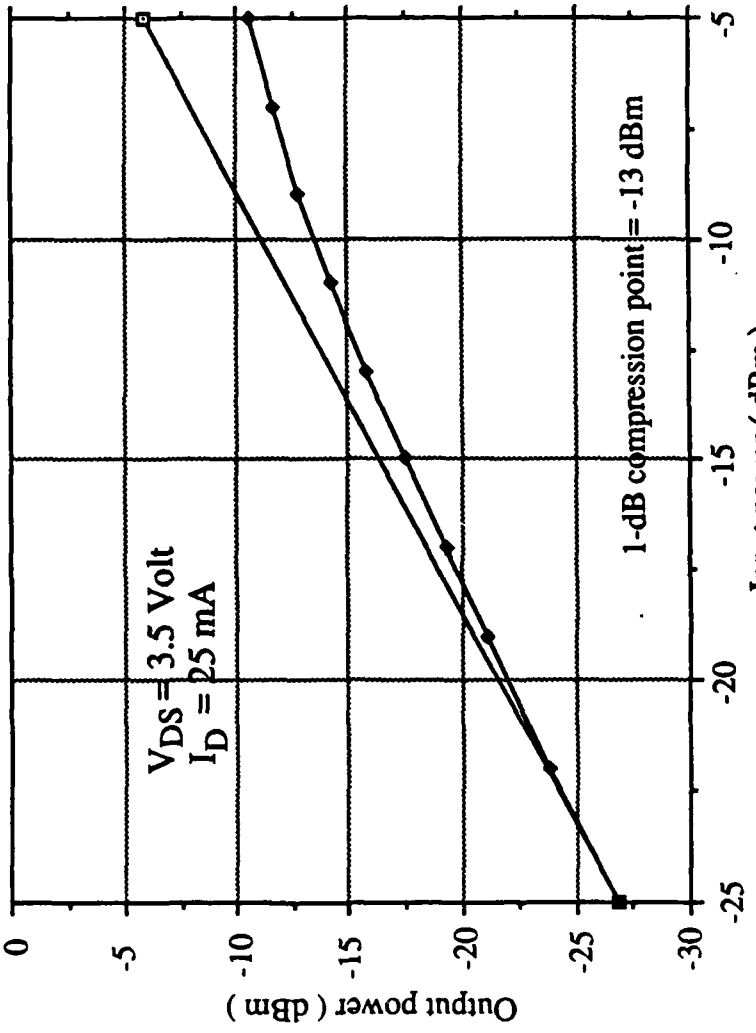

Fig. 3.4 The 1-dB compression curve of the one-pole active filter.

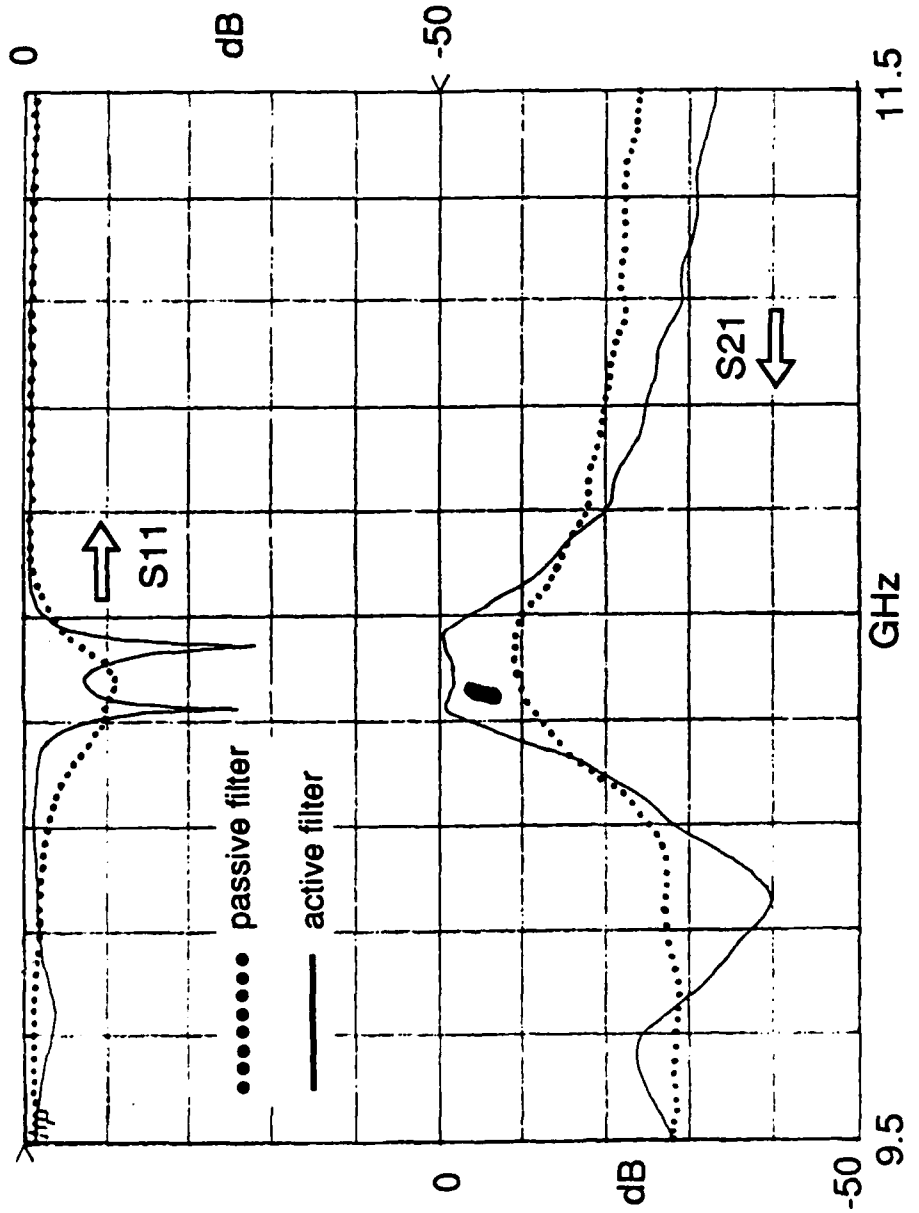

Fig. 3.5 The measured 2-pole filter performances.

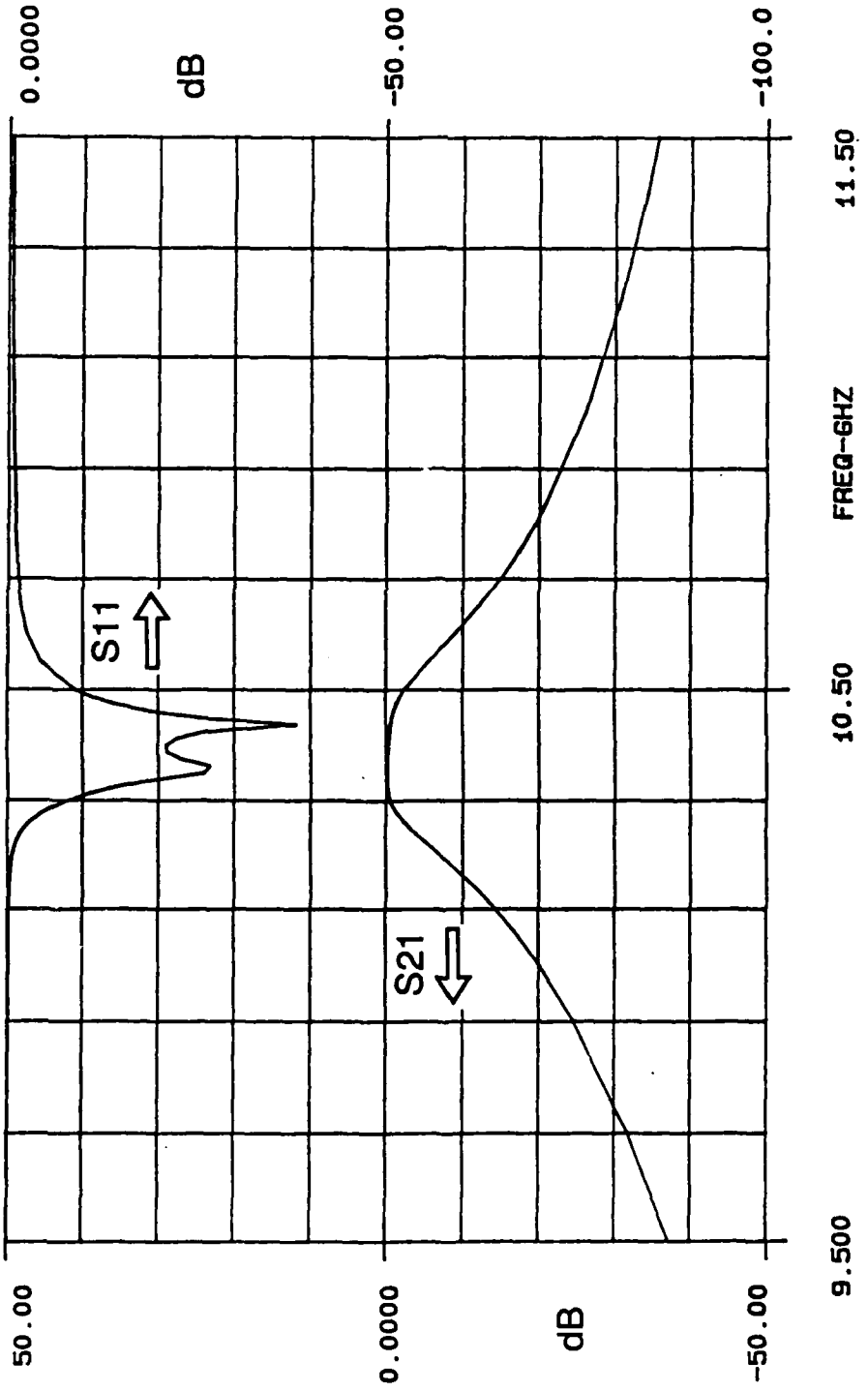

Fig. 3.6 The calculated 2-pole active filter performance.

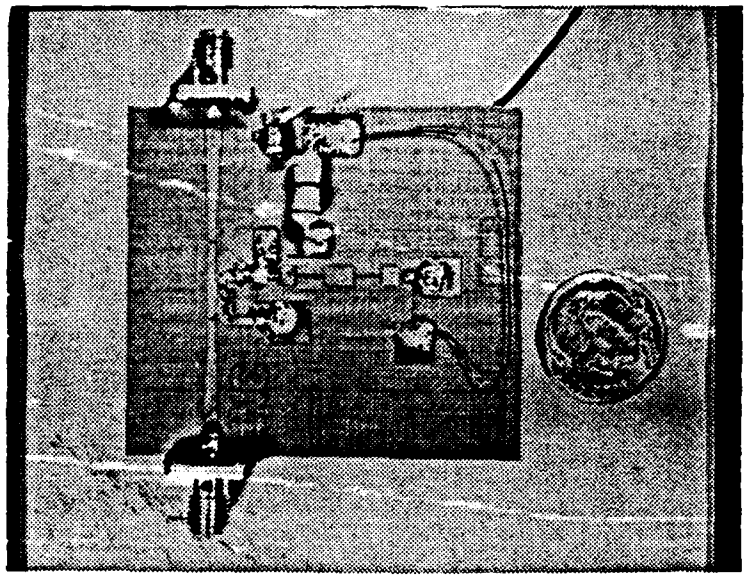

(a) The photograph of the 1-pole active filter.

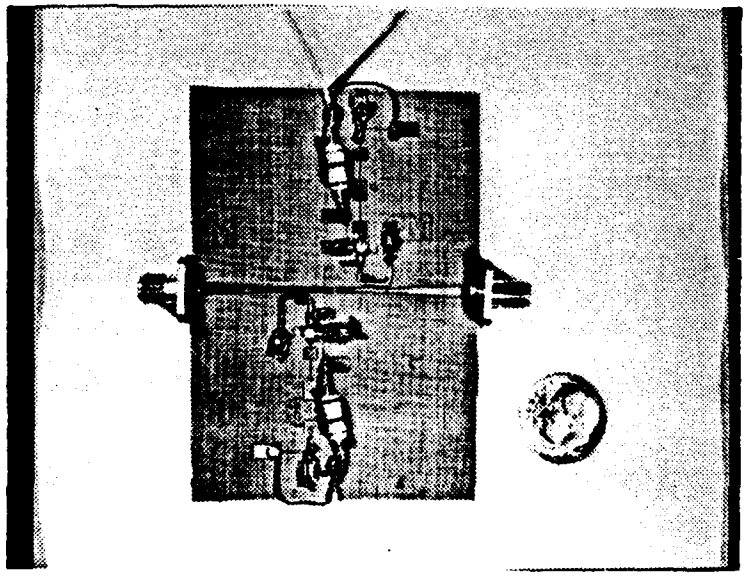

(b) The photograph of the 2-pole active filter.

Fig. 3.7 The photographs of end-coupled active filters.

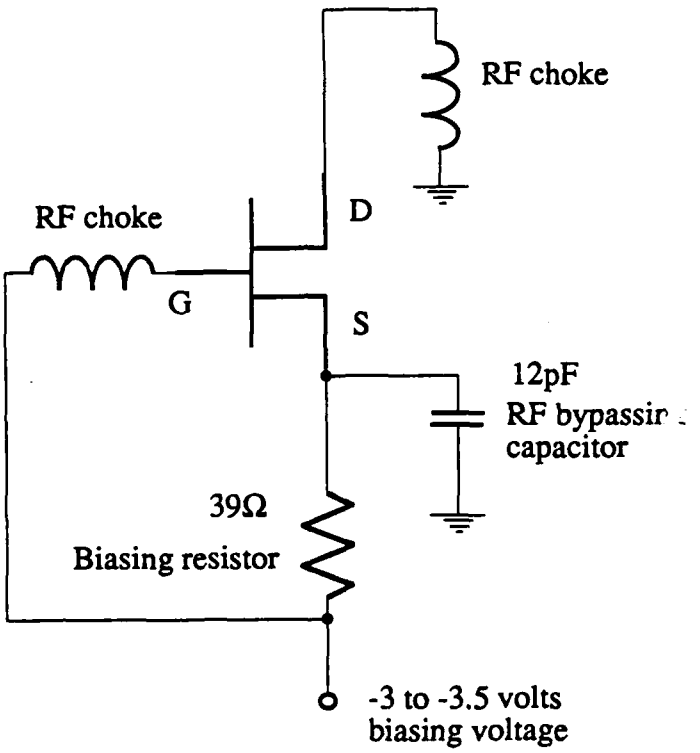

Fig. 3.8 MESFET DC biasing circuit.

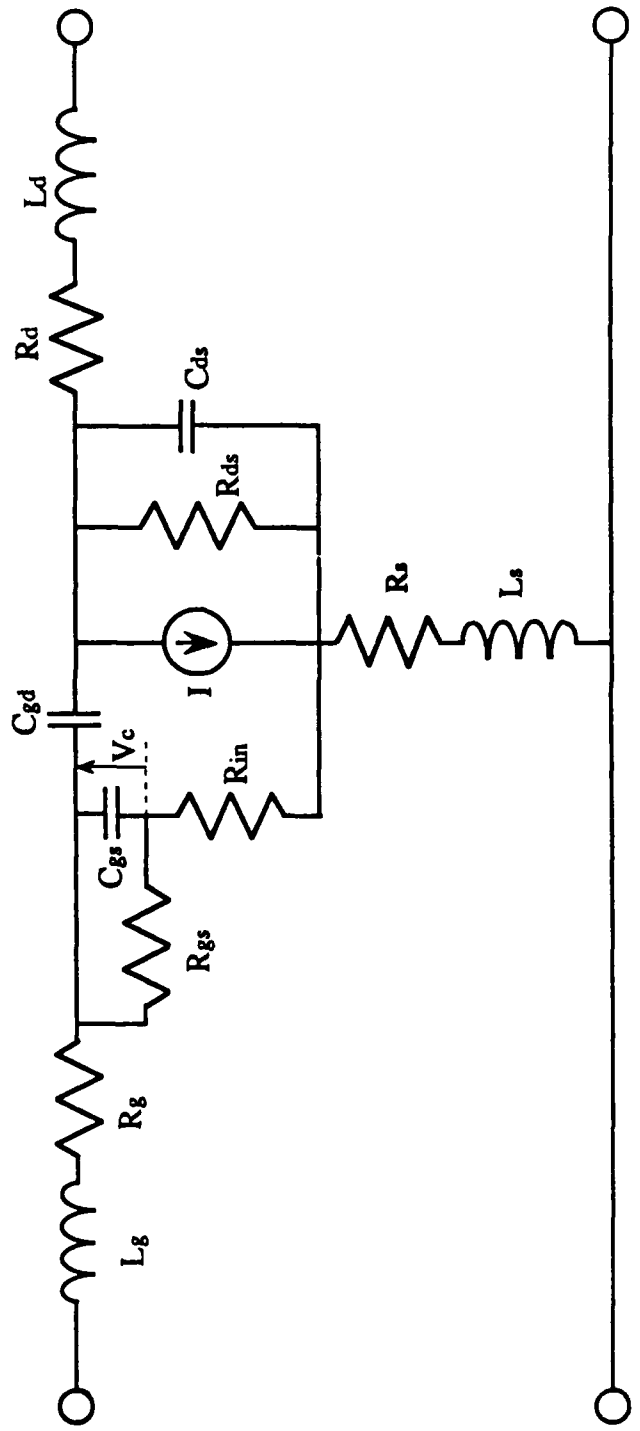

Fig. 3.9 The equivalent circuit of the MESFET used in MMIC active filter.

Parameters	Units	Typ.	Min.	Max.
g_m	mS	30	28.8	32.4
C_{gs}	pF	.264	.226	.308
C_{gd}	pF	.0365	.0323	.0416
C_{ds}	pF	.163	.129	.183
τ_t	pS	1.97	1.92	2.0
R_g	Ω	1.6		
R_{gs}	KΩ	17.87	17.8	18.3
R_{in}	Ω	7.29	6.73	8.3
R_s	Ω	1.14		
R_{ds}	Ω	378	364	387
R_d	Ω	5.06		
L_g	pH	40.64	26.7	64.0
L_s	pH	2.0	1.975	2.022
L_d	pH	59.0	57.15	61.55

Table. 3.2 The Hughes Co. MESFET parameters.

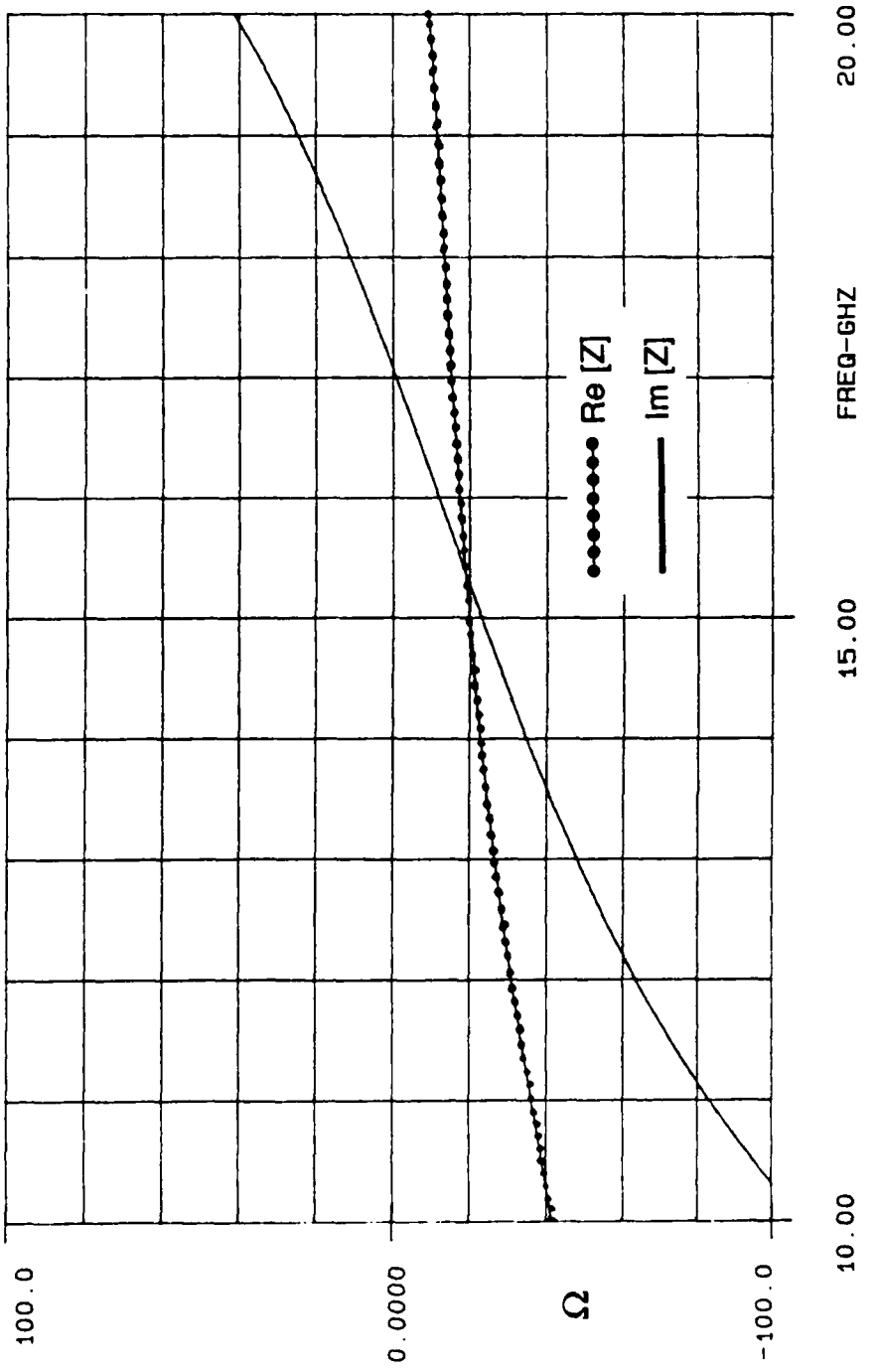

Fig. 3.10 Calculated negative resistance circuit performance.

(1) The minimum line width is 10 microns.

(2) The minimum gap width is 5 microns.

(3) The via hole is dry etched with diameter of 60 microns. The dry etched via holes have same diameter in front and back surfaces.

(4) The dielectric material for the capacitor is silicon nitride. The capacitance per unit area is 282 pF/mm^2 .

(5) The thickness of the gold conductor varies from 1.5 microns to 6 microns. In the active filter, we chose a metal thickness of 3 microns.

The MMIC active filter is designed to have a 3-dB bandwidth of 70 MHz at 17 GHz center frequency. The circuit layout is shown in Fig. 3.11, and the computer simulated performance is shown in Fig. 3.12. In this case, the MESFET uses separate gate and drain bias which are applied to two by-pass capacitors shown in Fig. 3.11.

In this chapter, an end-coupled active bandpass filter structure has been introduced. The design procedures have also been outlined. Special treatment for accurate tank circuit loss has been developed for accurate computer simulation of the active filter circuit. Based on these procedures, two MIC active filters were designed and fabricated. The measured performance of the MIC active filters shows apparent improvement in the passband region, and also shows good agreement with calculated results. The design procedures can be directly used in MMIC design. One example MMIC active filter has been designed. The computer simulated result of the MMIC

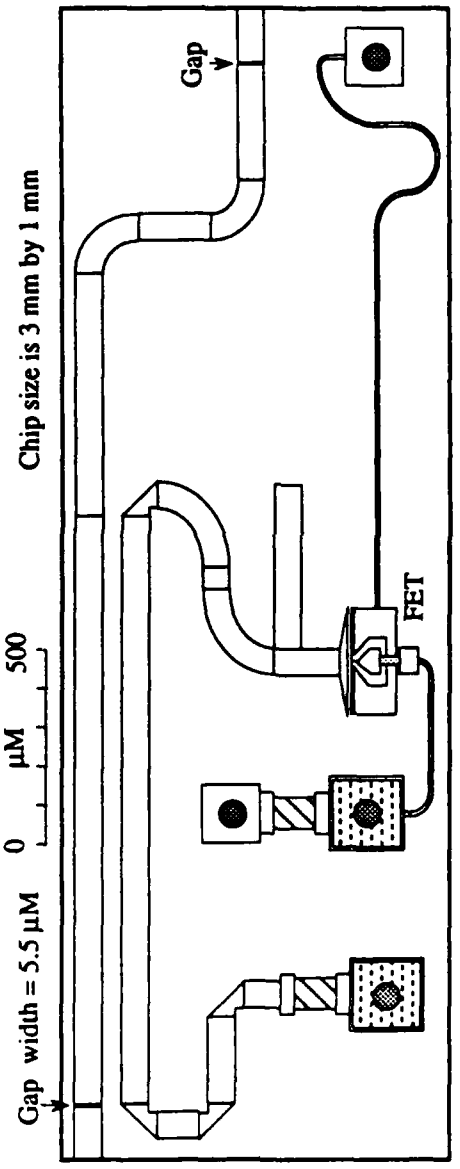

Fig. 3.11 MMIC layout of a 1-pole active filter.

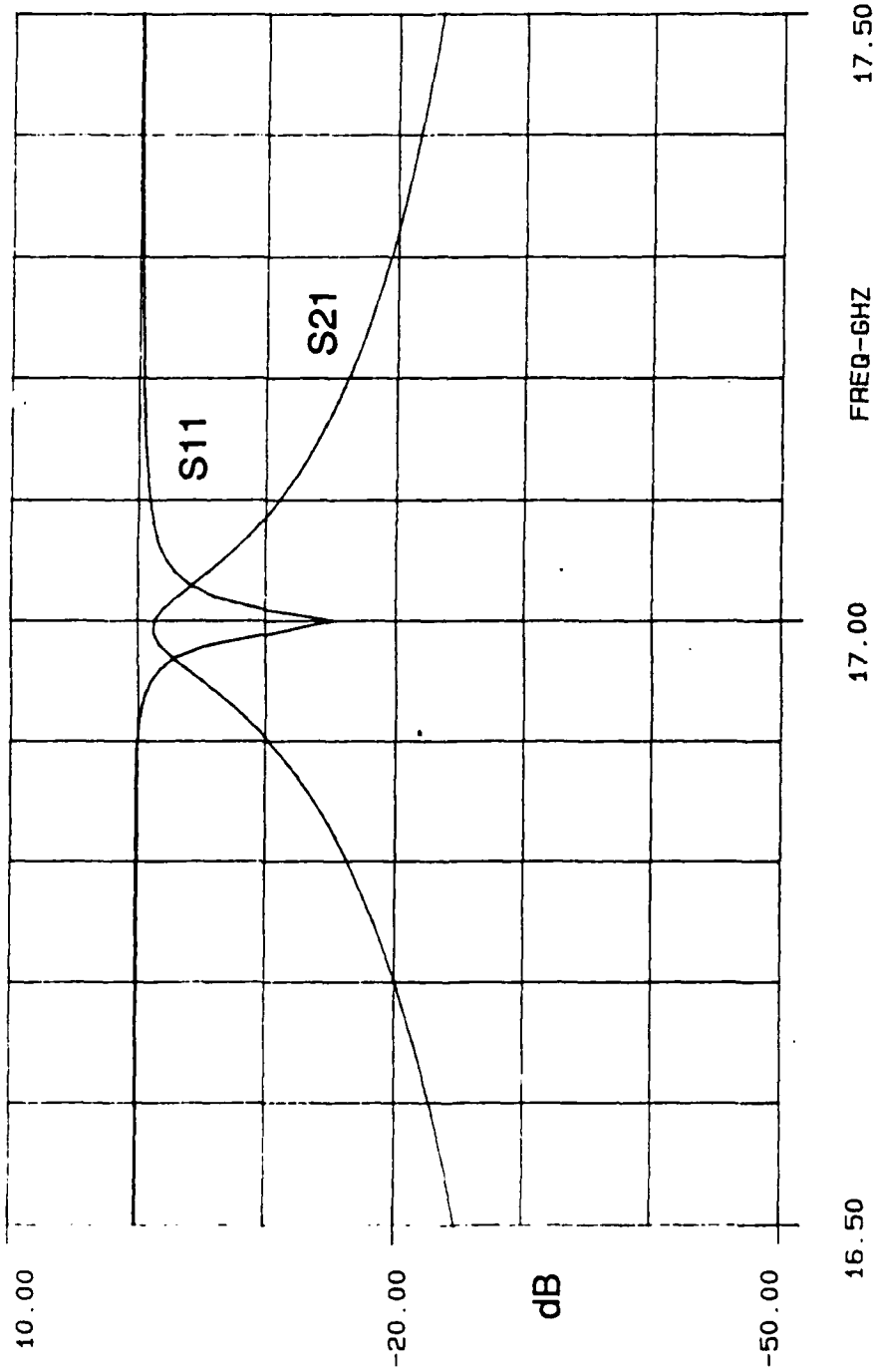

Fig. 3.12 Calculated MMIC 1-pole active filter performance.

filter shows significant increasing of the tank circuit unloaded Q value. This end-coupled filter structure is suitable for narrowband case especially for bandwidth less than 1%.

CHAPTER 4: MODERATE BANDWIDTH ACTIVE FILTERS

The bandwidth of the end-coupled active band pass filter introduced in previous chapter is very narrow. The maximum bandwidth of this kind of filter depends on the substrate thickness and dielectric constant, the center frequency, the number of poles, the passband ripple, the tank microstrip line characteristic impedance, and fabricating limitations. For instance, the smallest gap width of a MMIC circuit is about 5 microns. Based on this limit, if a 2-pole 0.1 dB ripple Chebyshev filter with center frequency 12 GHz is fabricated on a 100 micron thick GaAs substrate, the maximum bandwidth is 0.1%. This bandwidth limits the application of the active filter.

In order to broaden the bandwidth, a modified end-coupled active filter structure is introduced in this chapter. The coupled resonator filter disscussed in this report is constructed by tanks and coupling structures. The most strongly coupled tanks in the filter of this type are the first and last tanks. If the first and the last coupling structures are changed from microstrip gaps to microstrip quarter-wavelength parallel coupled lines, the bandwidth of the filter increases by a factor of 5 to 20. For example, using the new structure, the previously mentioned MMIC filter shows a bandwidth of up to 2% which is an improvement of a factor of twenty.

The modified end-coupled filter is shown in Fig. 4.1. The first and the last tanks in Fig. 4.1 are still exposed to outside. Therefore, the negative resistance circuits in the first and the last tanks are not influenced by these new coupling

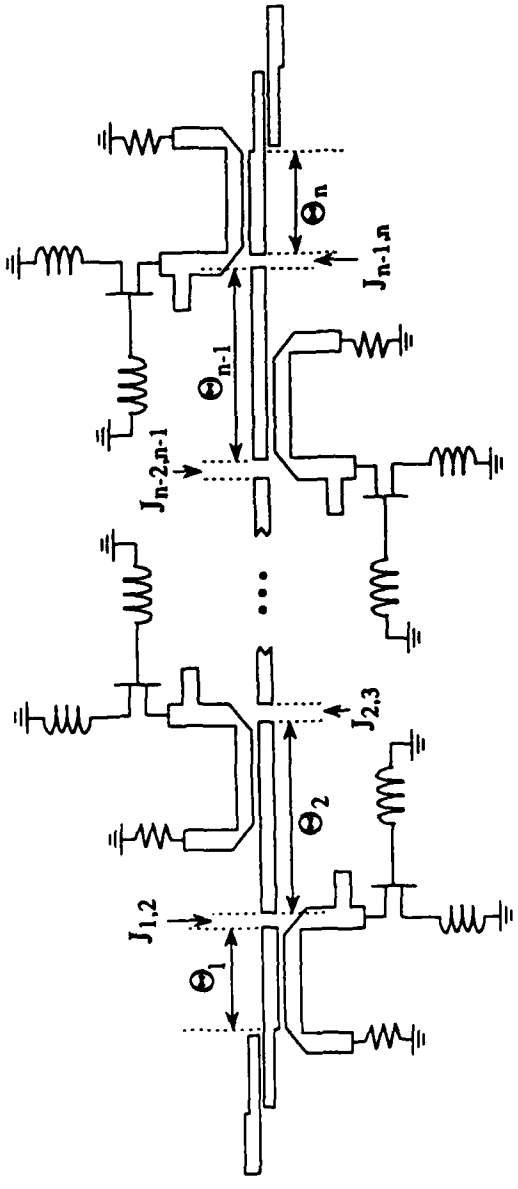

Fig. 4.1 The modified end-coupled active filter.

structures. This modified filter is a combination of end-coupled filter and parallel-coupled filter. The design equations are given by Eqs. 4.1 and Eqs. 4.2.

$$(Z_{oe})_{j,j+1} = \frac{1}{Y_0}\left[\, 1 + \frac{J_{j,j+1}}{Y_0} + \left(\frac{J_{j,j+1}}{Y_0}\right)^2 \right] \tag{4.1a}$$

$$(Z_{oo})_{j,j+1} = \frac{1}{Y_0}\left[\, 1 - \frac{J_{j,j+1}}{Y_0} + \left(\frac{J_{j,j+1}}{Y_0}\right)^2 \right] \tag{4.1b}$$

where j = 0 or n, and Z_{oe} and Z_{oo} are the even and odd mode impedances of the first and the last coupled-line sections.

$$\frac{B_{j,j+1}}{Y_0} = \frac{\frac{J_{j,j+1}}{Y_0}}{1 - \left(\frac{J_{j,j+1}}{Y_0}\right)^2} \tag{4.1c}$$

where j = 1, 2,..., n-1. Substituting Eqs. 4.1 into Eqs 3.1, the gap width $s_{j,j+1}$ and gap equivalent line extention $\Delta_{g_{j,j+1}}$ are obtained. The electrical length of each lines defined in Fig. 4.1 are given by Eqs. 4.2. In these equations, the equivalent line extension $\Delta_{g_{j,j+1}}$ is tanken into account.

$$\theta_1 = \frac{\pi}{2} - \frac{1}{2}\left[\, \tan^{-1}\left(\frac{B_{1,2}}{Y_0}\right) \right] - 2\pi\left(\frac{\Delta_{g\,1,2}}{\lambda_g}\right) \tag{4.2a}$$

$$\theta_j = \pi - \frac{1}{2}\left[\tan^{-1}\left(\frac{B_{j-1,j}}{Y_0}\right) + \tan^{-1}\left(\frac{B_{j,j+1}}{Y_0}\right)\right] - 2\pi\left(\frac{\Delta_{g\,j-1,j} + \Delta_{g\,j,j+1}}{\lambda_g}\right) \qquad (4.2b)$$

where j = 2, 3, 4,..., n-1, and

$$\theta_n = \frac{\pi}{2} - \frac{1}{2}\left[\tan^{-1}\left(\frac{B_{n-1,n}}{Y_0}\right)\right] - 2\pi\left(\frac{\Delta_{g\,n-1,n}}{\lambda_g}\right) \qquad (4.2c)$$

To verify the validity of the new structure, a 3-pole passive bandpass filter is designed and fabricated. The filter is designed to have 12% bandwidth at 10 GHz and with 0.1 dB passband ripples. Fig. 4.2 and Fig.4.3 show the measured and computer simulated performance curves of the 3-pole filter.

Based on the new structure, three active filters are designed and fabricated. Table. 4.1 shows the filter parameters. The negative resistance circuits used in these filters are shown Fig. 2.10b. The inductors are realized by 4-mil-width high impedance microstrip lines. The length of these high impedance lines are 10 mils for the gate feed back inductor and 40 mils for the source feedback inductor. The MESFETs are biased in an I_{Dss} condition.

The filters transmission and reflection responses were measured by the HP-8510 network analyzer. The third order interception point of the filters are also measured. The measured data is shown in Table 4.1. The interception point data are important for evaluating the useful dynamic range of the active filters.

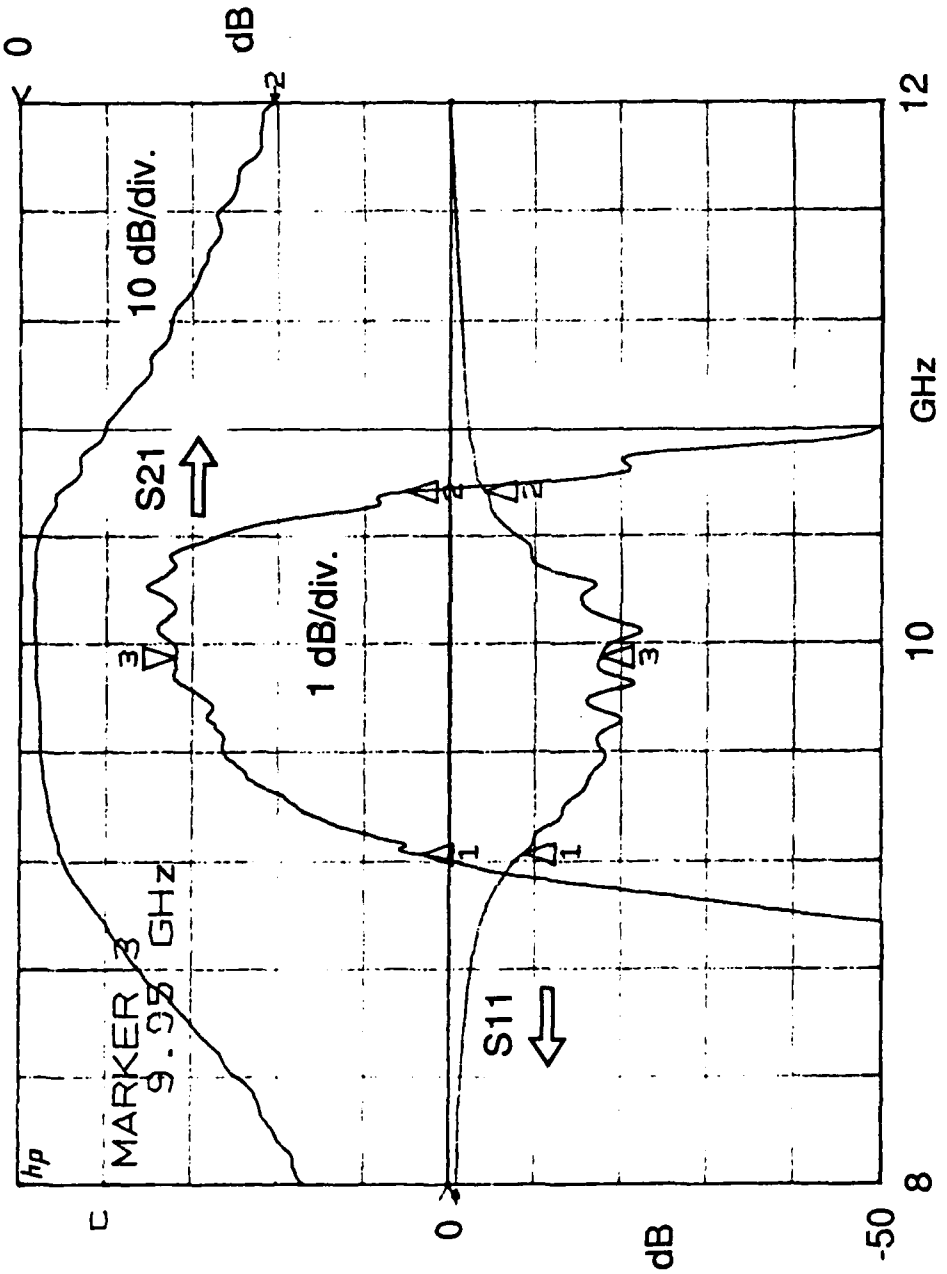

Fig. 4.2 Measured 3-pole modified end-coupled filter performance.

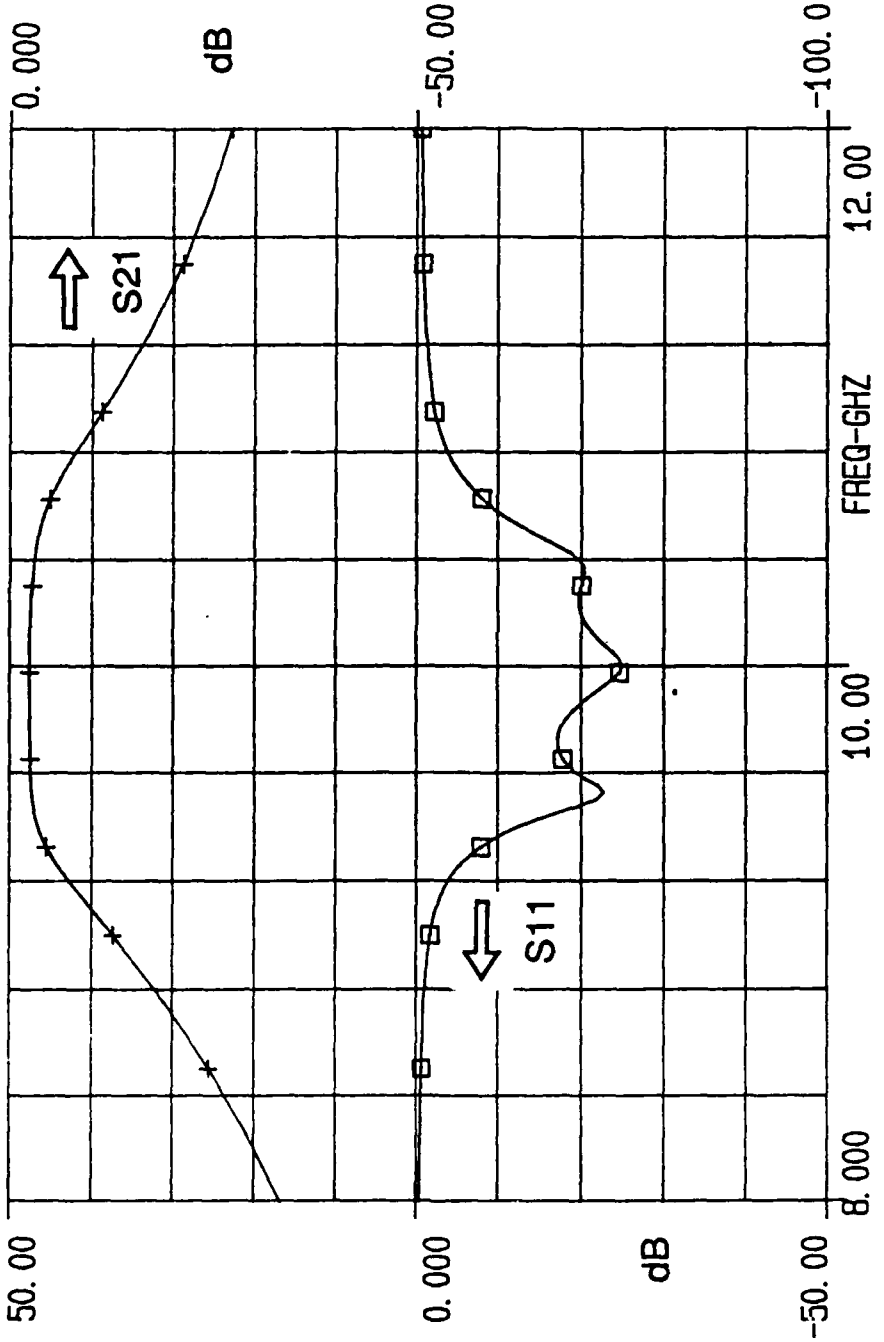

Fig. 4.3 Calculated 3-pole modified end-coupled filter performance.

Spec. \ Filter No.	Filter No.1	Filter No.2	Filter No.3
Type of design	Chebyshev	Chebyshev	Chebyshev
Center frequency	9.05 GHz	9.26 GHZ	9.07 GHZ
Relative bandwidth † corresponding to L_{Ar}	1.75 %	2.4 %	7.5 %
Passband ripple	0.1 dB	0.1 dB	0.3 dB
Number of poles	2	2	2
Substrate thickness	29.5 mil	29.5 mil	29.5 mil
Substrate ε_r	2.55	2.55	2.55
Smallest gap width *	27 mil at 1st gap	23.8 mil at 1st gap	4.1 mil at 2nd gap
System impedance **	82 Ω	82 Ω	82 Ω
3rd-order inter-ception point	- 4 dBm	- 4 dBm	+ 10 dBm

† : The L_{Ar} is the frequerncy that the loss equals to ripple value and begins to roll-off.

* : The first gap is the parallel coupled line gap.

** : The non-50 Ω system impedance is tapered to 50 Ω at input and output.

Table 4.1 The parameters of the modified end-coupled active filters.

Fig. 4.4 show photographs of filters #1 and #3. The measured filter performances are shown in Fig. 4.5 to Fig. 4.7. The original end-coupled active filter is limited to a bandwidth of 1.25% corresponding to a gap width of 4 mils at the first gap. However, the modified active filter can have 7.5 % bandwidth with the same gap width, namely 4 mils, at the second gap. Each of the filters shows about 1dB passband insertion gain. Compared to the power turned-off case, the active filter shows a significant improvement in filter passband corner shape and in the passband return loss and insertion loss.

In this chapter, a modified end-coupled filter structure was introduced. The design procedures for this new structure were outlined. Based on this modified structure, the bandwidth of an active filter may be broadened by a factor of 5 to 20. Three example active filters have been designed and fabricated. The measured performances are in good agreement with the calculated result. The modified active filter may have more applications than the original end-coupled active filter described in Chapter. 3.

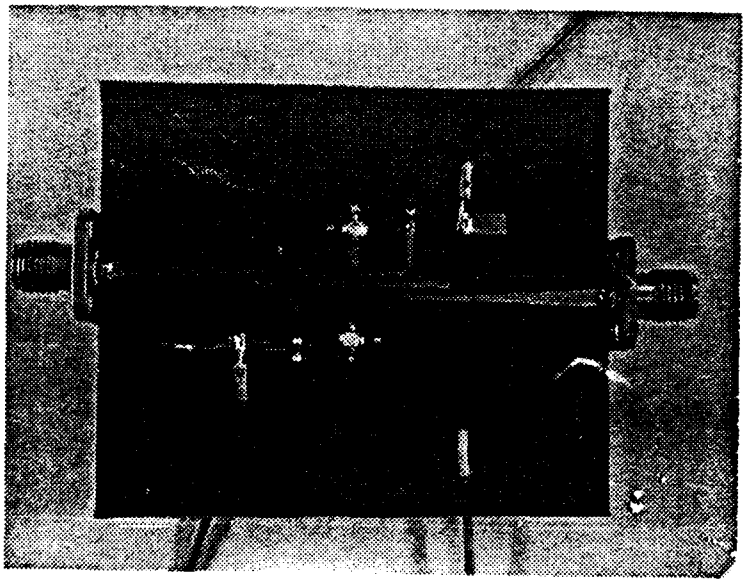

(a) The photograph of No.1 active filter.

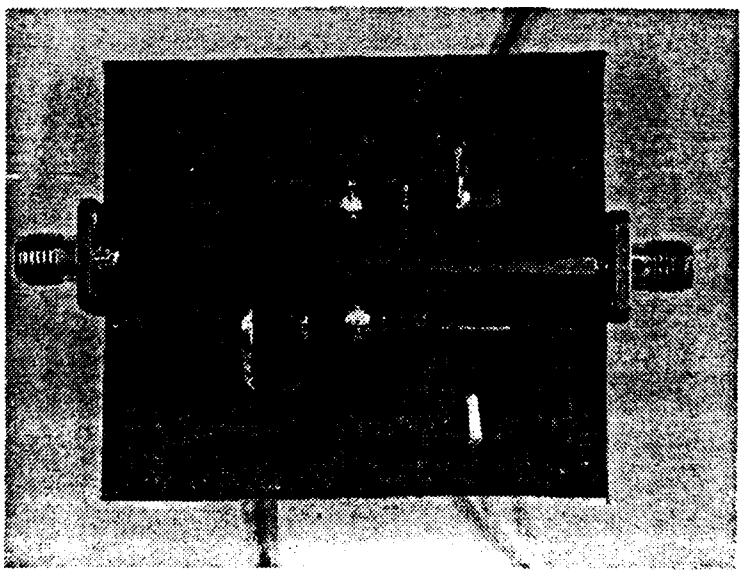

(b) The photograph of No.3 active filter.

Fig. 4.4 The photographs of modified end-coupled active filters.

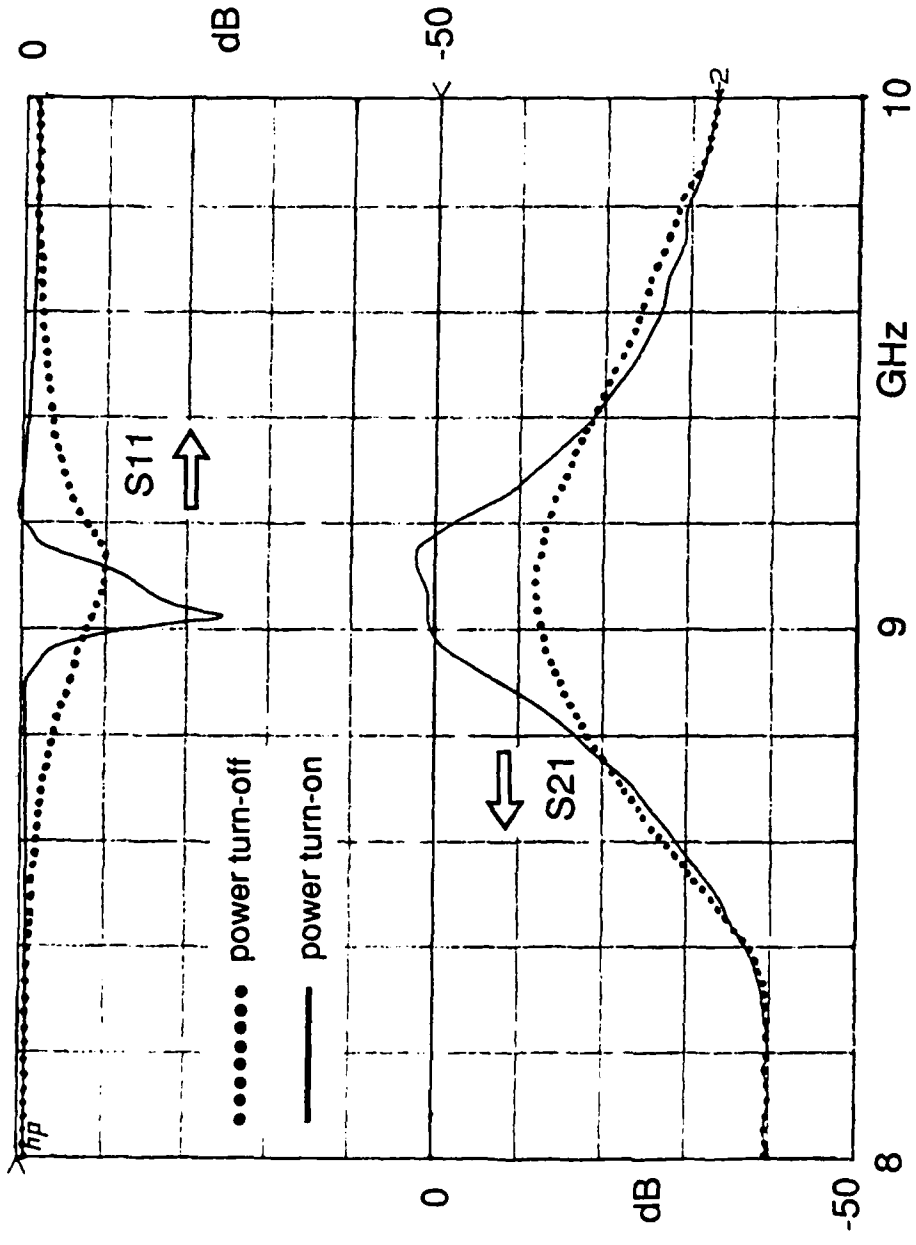

Fig. 4.5 Measured performance of No. 1 active filter.

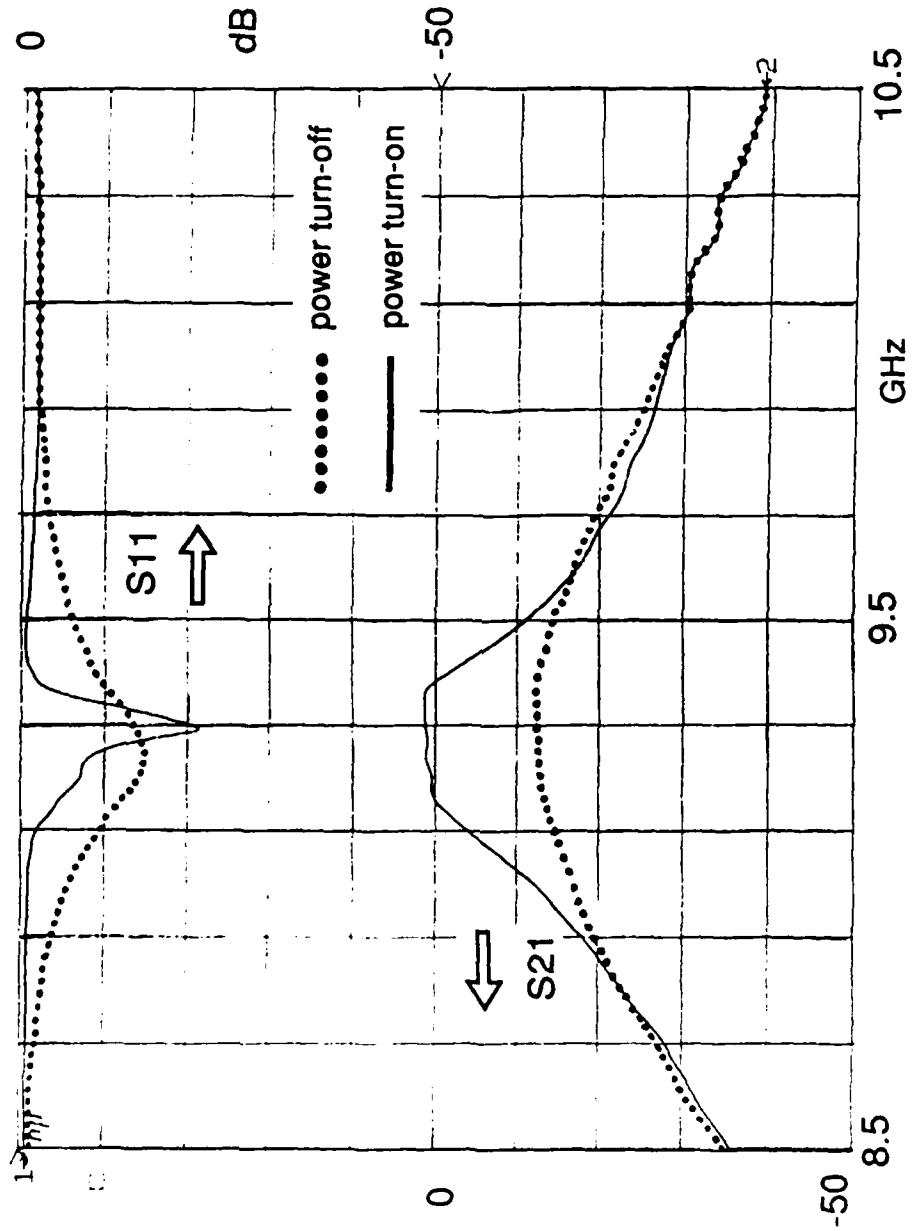

Fig. 4.6 Measured performance of No. 2 active filter.

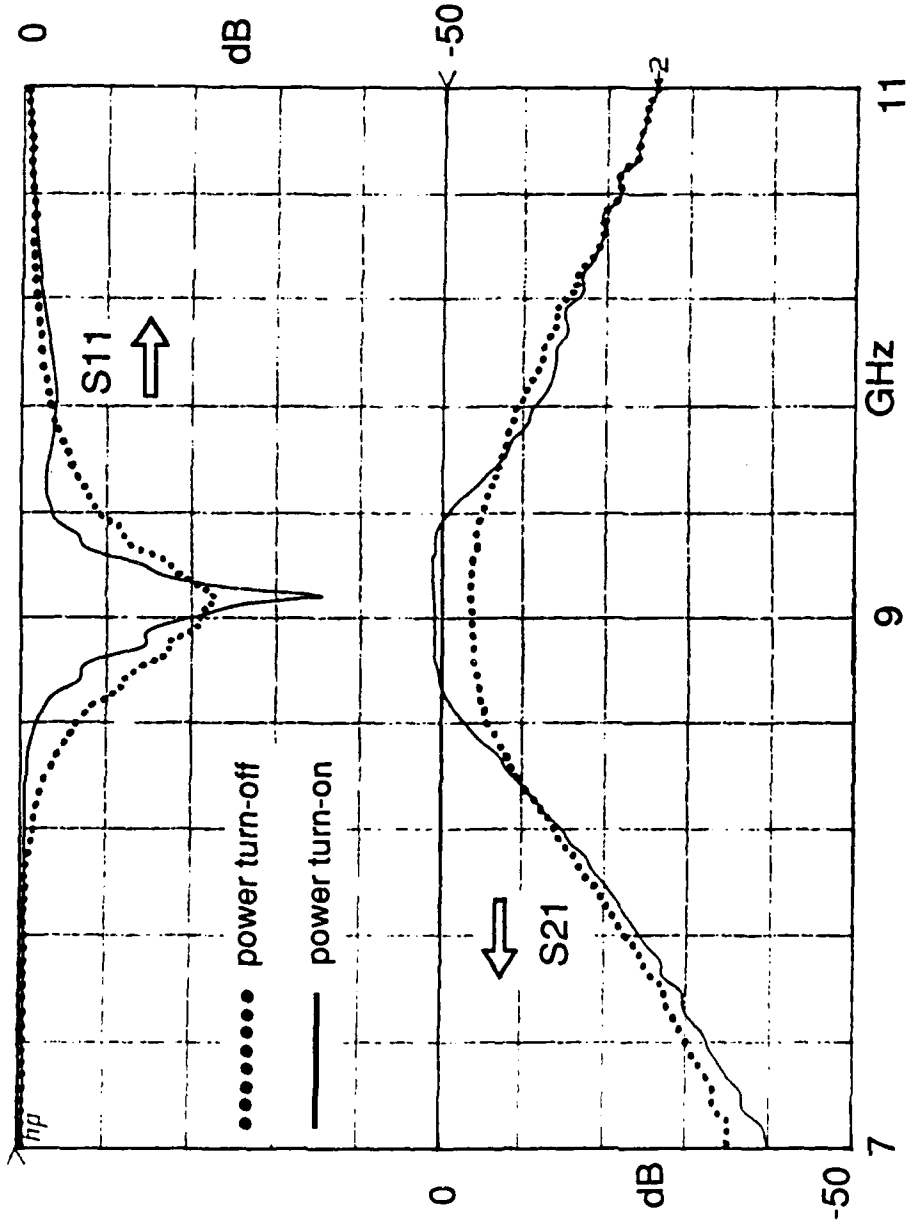

Fig. 4.7 Measured performance of No. 3 active filter.

CHAPTER 5: MODIFIED PARALLEL-COUPLED FILTER STRUCTURE FOR BROADBAND ACTIVE FILTERS

The parallel-coupled filter has been one of the most popular used filter structures for more than 30 years. This filter was first introduced by S. B. Cohn in 1958 [18]. This type of filter has many advantages such as easy design procedures, wide bandwidth range (from a few % to more than 40 %), planar structure. The filter performance is reasonably good compared to other planar circuit filters. One disadvantage is that when the bandwidth gets broader the upper stopband rejection is degraded. Nevertheless, it is still a good choice for broadband filters. Unfortunately, this filter structure is not applicable to the active filter described from Chapter 2 through Chapter 4. Because of the embedded tanks in this filter structure, the active circuit has no space to couple to the tanks. Fig. 5.1 shows the parallel-coupled filter structure.

In order to solve the embedded tank problem, a modified parallel-coupled filter structure is introduced. Fig. 5.2 shows the modified filter structure. The tanks are exposed to the outside so that the active circuit has space to couple to the tanks. Instead of the microstrip open-end effect in the traditional parallel-coupled filter, there are microstrip gaps in the new filter everwhere except for the first and the last couplers. However, the gap model developed in Chapter 3 can not be used in this case because that gap model is a special case (the input and the output line are aligned and with the same width), and it is difficult to apply to this offset gap case. However, these gaps are critical to the filter performance. Even now, there

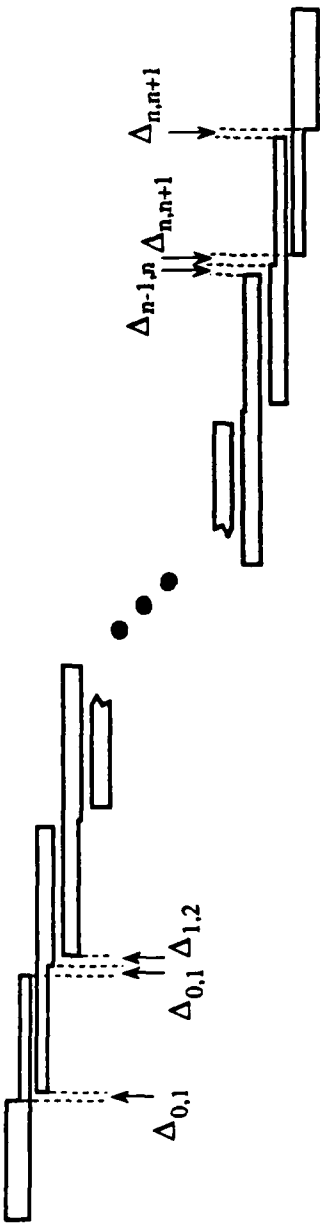

where $\Delta_{i,i+1}$ is the microstrip open-end pre-short.

Fig. 5.1 The traditional parallel-coupled filter with open-end pre-short.

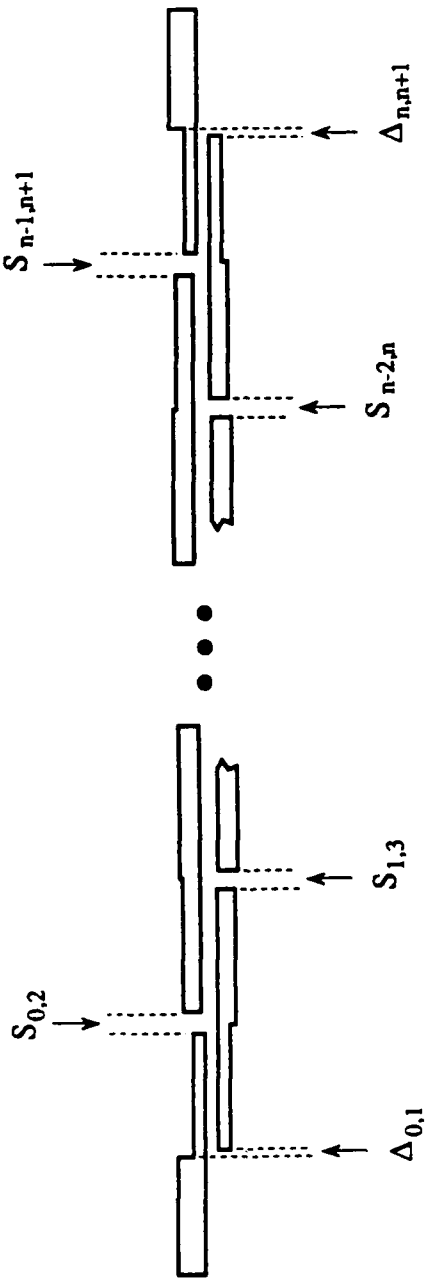

where $S_{i,i+2}$ is the offset gap.

Fig. 5.2 The modified parallel-coupled filter with offset gaps.

exists no good circuit model for this kind of gap. Here, a semi-empirical method is used. Using this semi-empirical method, the computer simulated filter performance is in good agreement with the measured performance.

In the case of the traditional parallel-coupled filter, there are two methods for treating the open-end of the quarter-wave coupler. Methods of treatment are shown in Fig. 5.3. The treatment method in Fig. 5.3a requires experience to obtain the optimal shape of rounded-end for best filter performance. Here, the treatment method in Fig. 5.3b is chosen. This method is the so called pre-short method. The length of pre-short, $\Delta_{i,i+1}$, is equal to the equivalent length extension of a microstrip line having the same physical dimensions. The equivalent length extension of an open-end microstrip was discussed in many papers [19-21]. Here, the curve fitting equation by R. Garge and I. J. Bahl [21] is chosen. Eqn. 5.1 shows the relation between the length extension and the microstrip line physical parameters.

$$\frac{\Delta_{i,i+1}}{h} = 0.412 \left(\frac{\varepsilon_{re} + 0.3}{\varepsilon_{re} - 0.258} \right) \left(\frac{u + 0.264}{u + 0.8} \right) \tag{5.1a}$$

where **u** is defined in Eq. 3.1a and ε_{re} is effective dielectric constant which is given by Eq. 5.1b through Eq. 5.1d [22].

$$\varepsilon_{re} = \frac{\varepsilon_r + 1}{2} \frac{\varepsilon_r - 1}{2} \left(1 + \frac{10}{u} \right)^{-a(u)\, b(\varepsilon_r)} \tag{5.1b}$$

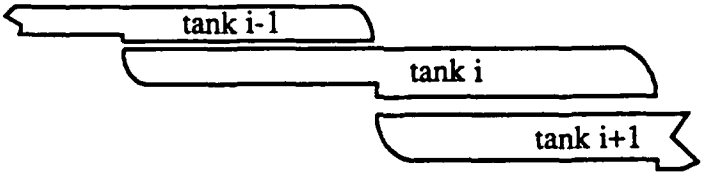

(a) The microstrip open-end treated by rounding the end.

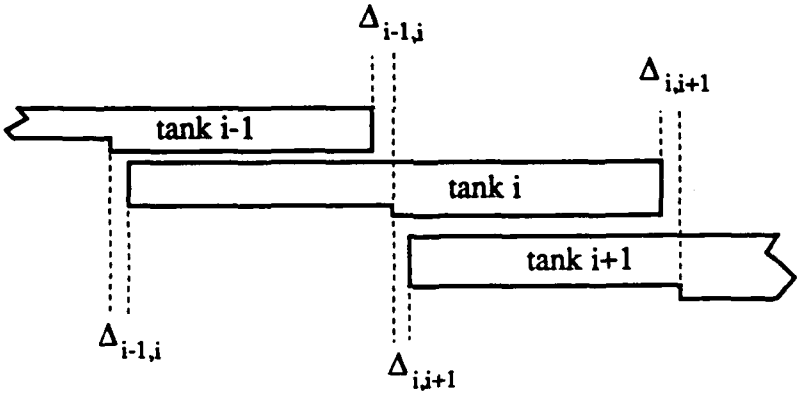

(b) Microstrip open-end treated by pre-short.

Fig. 5.3 Two treatment methods for microstrip open-end.

where ε_r is the substrate dielectric constant, and

$$a(u) = 1 + \frac{1}{49} \ln \left[\frac{u^4 + \left(\frac{u}{52}\right)^2}{u^4 + 0.432} \right] + \frac{1}{18.7} \ln \left[1 + \left(\frac{u}{18.1}\right)^3 \right] \qquad (5.1c)$$

$$b(\varepsilon_r) = 0.564 \left(\frac{\varepsilon_r - 0.9}{\varepsilon_r + 3} \right)^{0.053} \qquad (5.1d)$$

where the valid range of Eq. 5.1a is limited to $\mathbf{u} < 3$. The modified filter has two open-ends at the first and the last quarter-wave coupled lines as shown in Fig. 5.2. The Eqs. 5.1 is also used to calculate these open-ends in Fig. 5.2.

To analyze the modified filter response, the equivalent circuit model for the offset microstrip gap as shown in Fig. 5.4 is required. A semi-empirical method to determine the gap model is adopted. In Fig. 5.4, using the overlapped line width w_{eq} as the line width w_{strip} in Eqs. 3.1, the equivalent gap model may be obtained. Including this gap model into the Touchstone™ simulator, the optimal performance of the modified filter may be achieved.

As mentioned above, the upper stopband rejection of a traditional parallel-coupled filter degrades as the bandwidth of the filter gets broader. The modified parallel-coupled filter improves the upper stopband rejection by at least 15 dB.

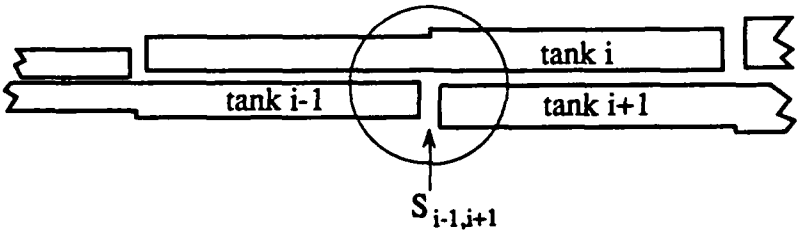

(a) The gaps in modified parallel-coupled filter.

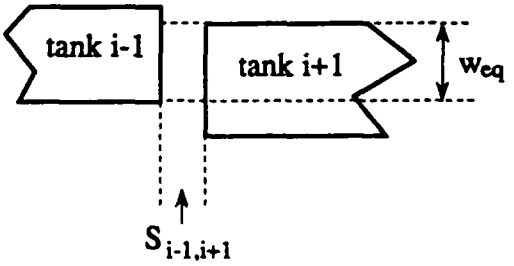

(b) Detailed view of the circle area in (a),
where w_{eq} is the equivalent line width.

Fig. 5.4 The treatment of offset gap in modified parallel-coupled filter.

Theoretically, the parallel-coupled filter has a serious problem in frequency asymmetry when the relative bandwidth is greater than a few percent. For a traditional parallel-coupled filter, the lower frequency side has steeper roll-off than the upper frequency side. The modified parallel-coupled filter improves the situation. Compared to the traditional filter, the modified filter shows less steep roll-off in the lower frequency side and steeper roll-off in the higher frequency side. This greatly improves the frequency response asymmetry phenomenon.

To verify the performance improvement several filters were built. The filter parameters are shown in Table 5.1. The filters were fabricated on two kinds of substrates: one is woven type PTFE substrate with thickness 29.5 mil and dielectric constant 2.55, the other is Duroid™ 6010 (a brand name of Rogers Co.) with thickness 25 mil and dielectric constant 10.2. These two dielectric constant values cover those most commonly used in microwave substrates.

The filters were measured by a HP-8510 network analyzer. The filter under test was shielded by foam type wave absorber to eliminate unwanted radiation which may influence the performance curve.

Fig. 5.5 shows the calculated performance of filter #1. Fig. 5.6 shows measured performance of filter #1. Comparing Fig. 5.5 to Fig. 5.6, the two results are well matched. It shows that CAD of this modified filter is possible.

Fig. 5.7 to Fig. 5.10 show the performance curves of filters #2 to #5. These figures show that the upper stopband rejection is improved by at least 15 dB. The figures also show the improvement of the frequency response symmetry. It can be

Spec. \ Filter no.	No. 1	No.2	No.3	No.4	No.5
Type of design	Cheby.	Cheby.	Cheby.	Cheby.	Cheby.
Center freq.	8 GHz	8 GHz	10 GHz	10 GHz	10 GHz
% bandwidth	25 %	25 %	40 %	40 %	40 %
Passband ripple	0.1 dB	0.1 dB	0.1 dB	0.1 dB	0.1 dB
Substrate ε_r	10.2	2.55	10.2	2.55	2.55
Substrate thik.	25 mil	29.5 mil	25 mil	29.5 mil	29.5 mil
No. of poles	3	3	3	3	4
S_{02} †	7 mil	12 mil	5 mil	15 mil	25 mil
S_{13} †	10 mil	17 mil	5 mil	15 mil	30 mil
Δ_{01} †	6.2 mil	9.7 mil	5.3 mil	10.3 mil	10.5 mil
Δ_{12} †	7.1 mil	11 mil	6.2 mil	11.4 mil	11.7 mil
Δ_{23} †	-	-	-	-	12.1 mil
Sys. impedance*	50 Ohm	82 Ohm	50 Ohm	60 Ohm	60 Ohm

† : Defined in Fig. 5.1 and Fig. 5.2.

* : The non-50 Ohm system impedance is tapered to 50 Ohm at input and output.

Table 5.1. The filter design parameters.

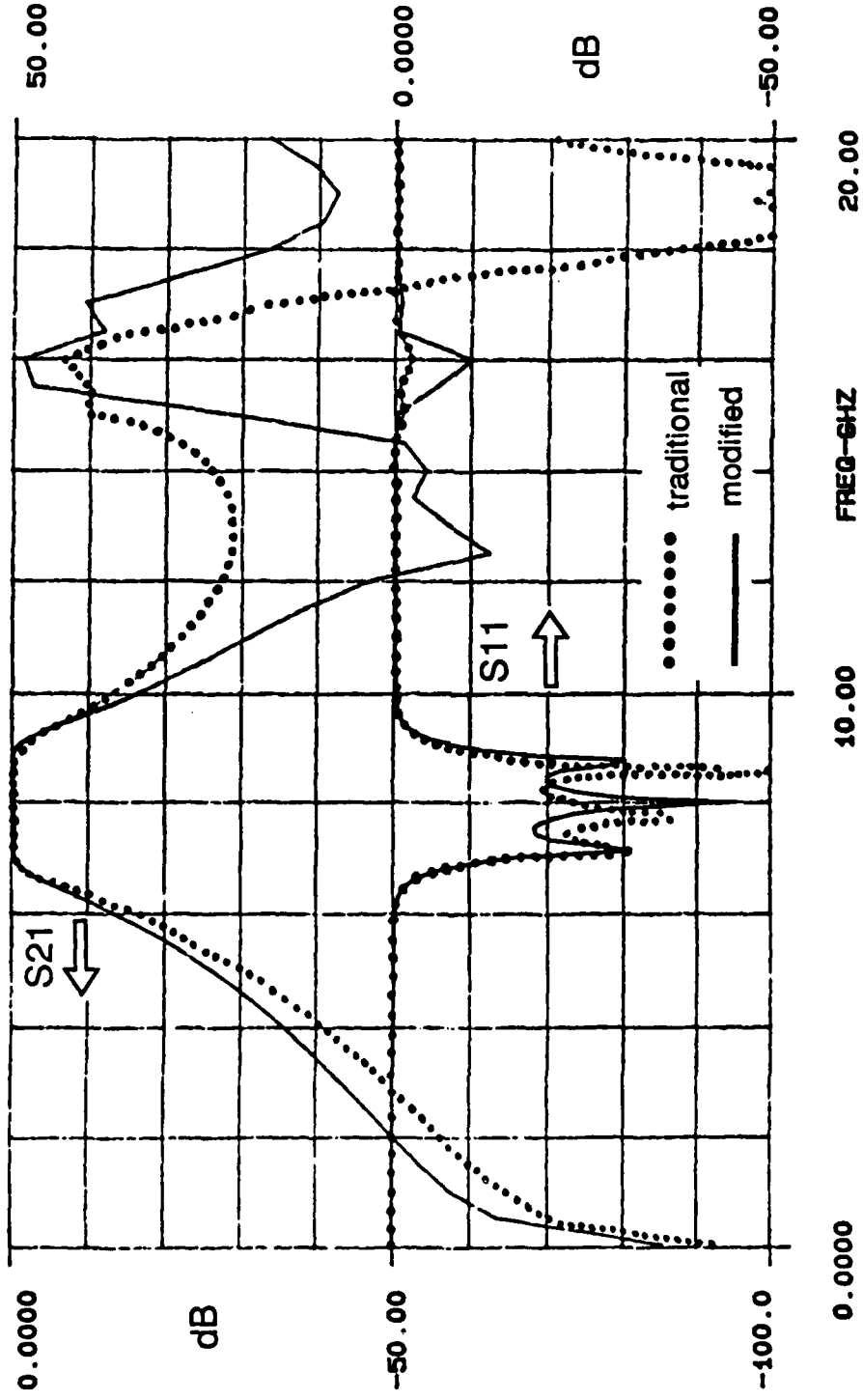

Fig. 5.5 Calculated performance of filter #1.

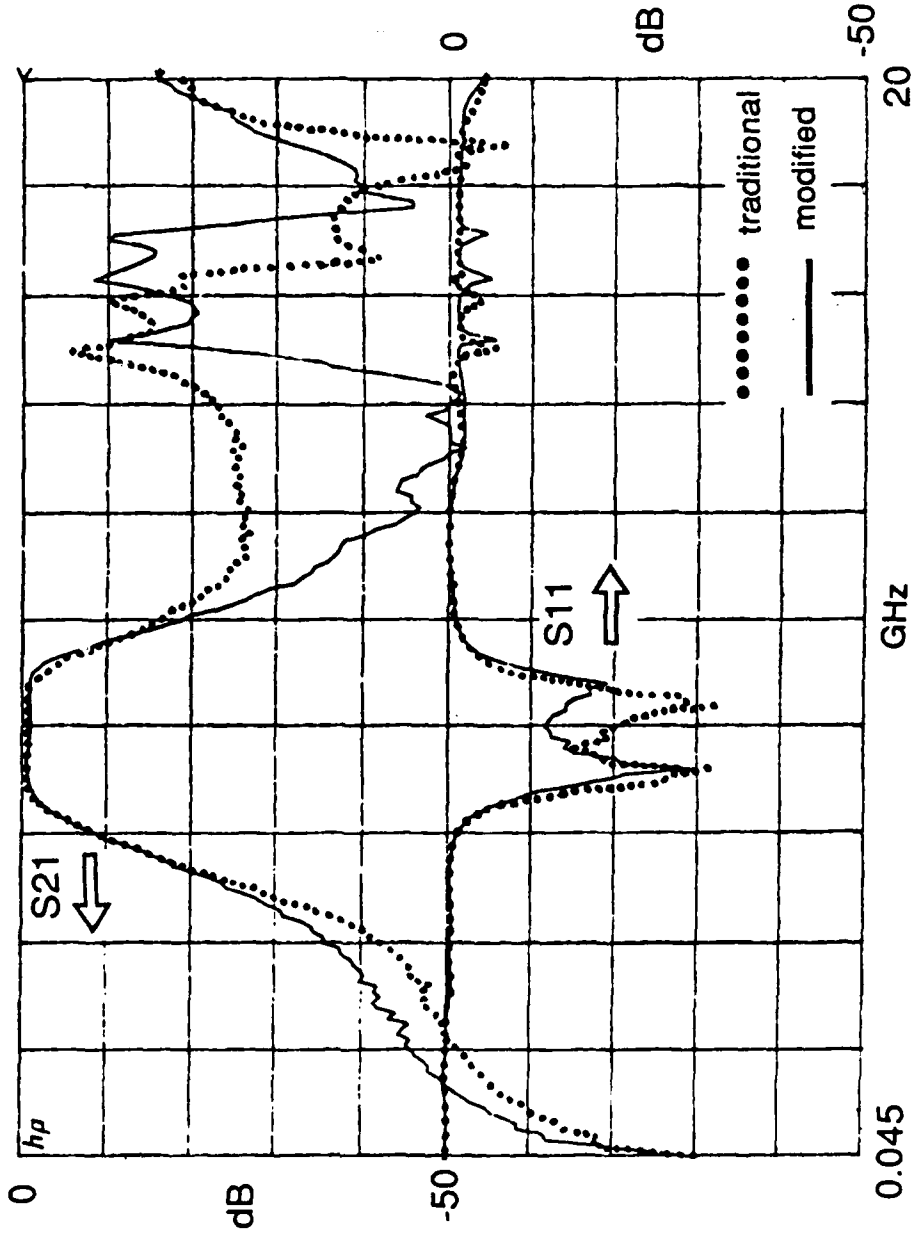

Fig. 5.6 Measured performance of filter #1.

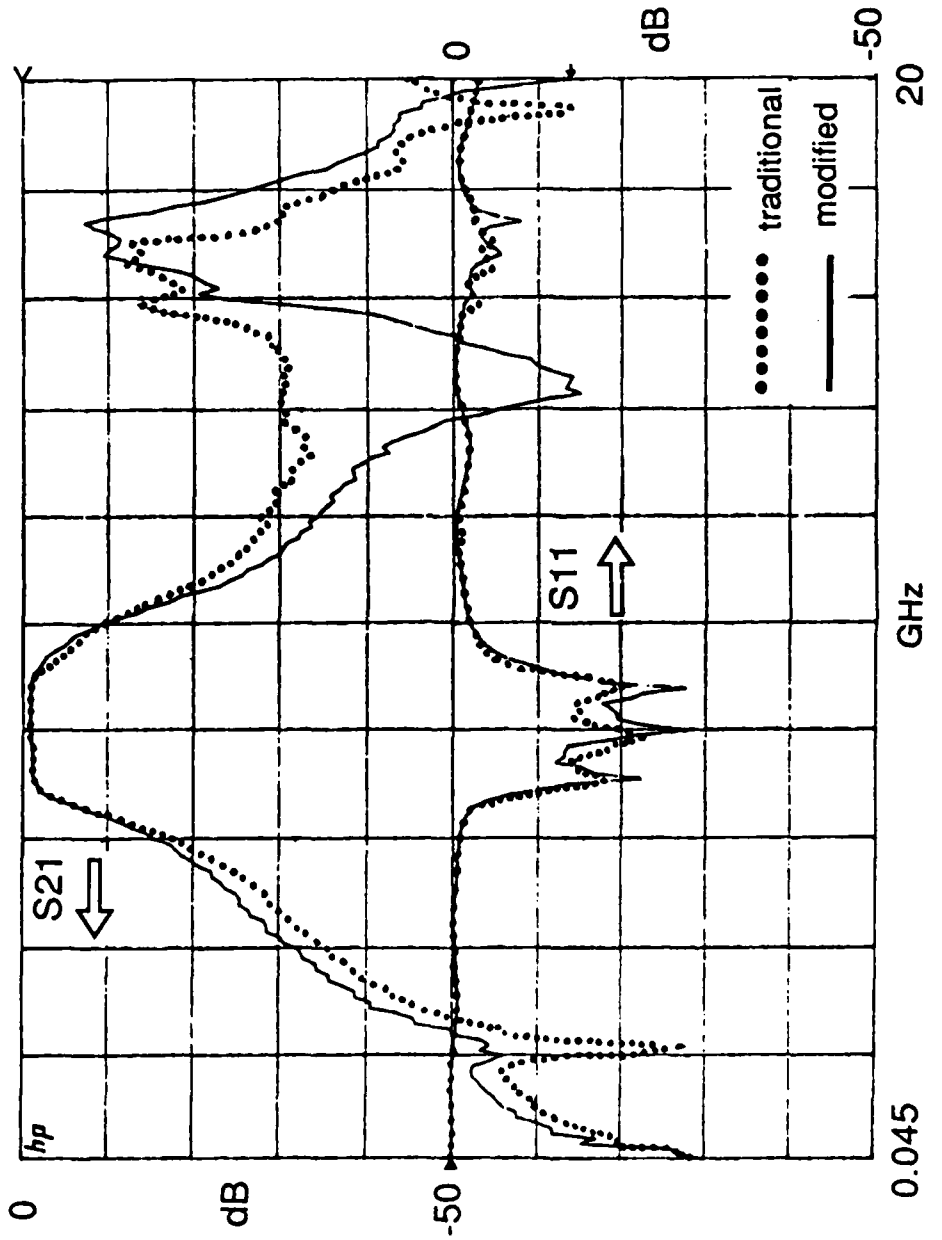

Fig. 5.7 Measured performance of filter #2.

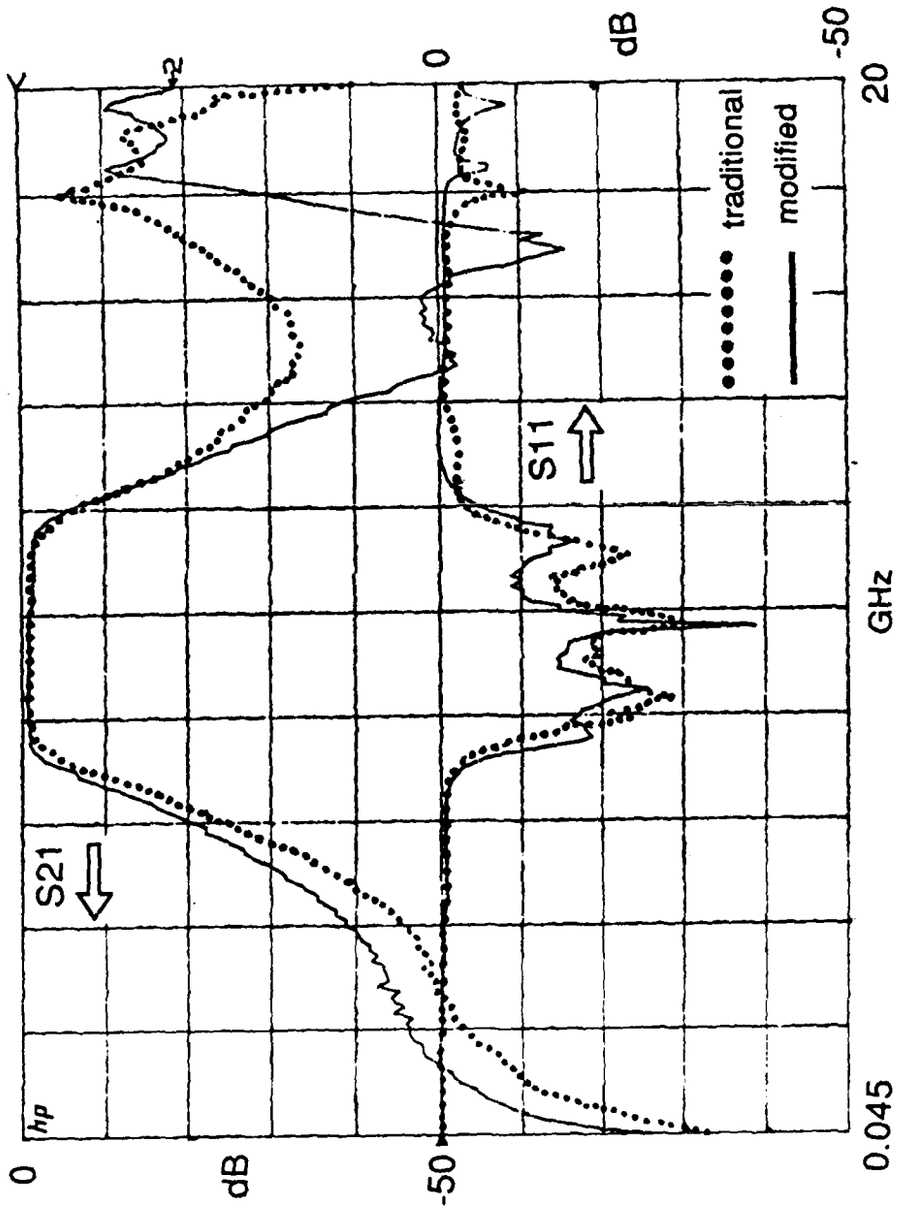

Fig. 5.8 Measured performance of filter #3.

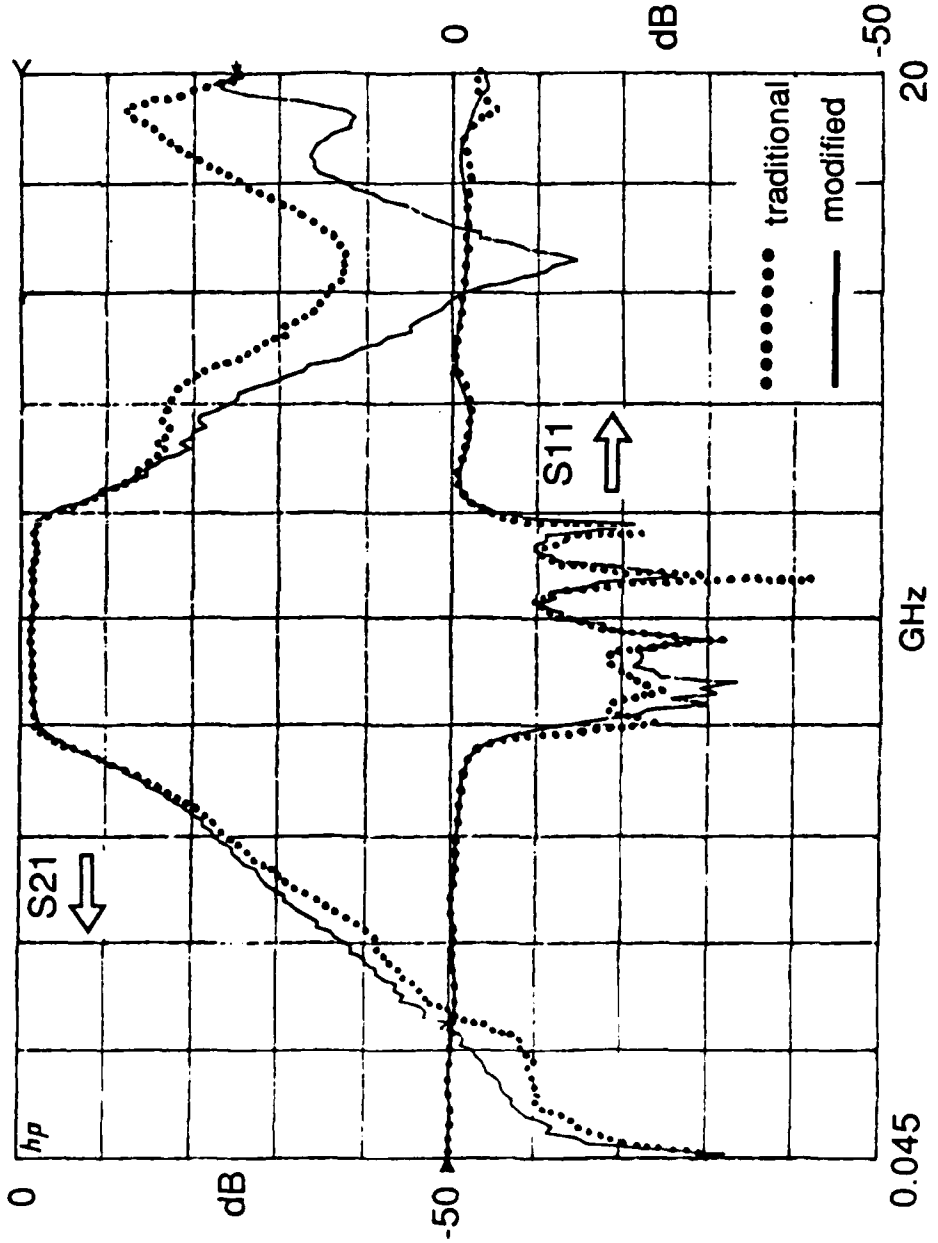

Fig. 5.9 Measured performance of filter #4.

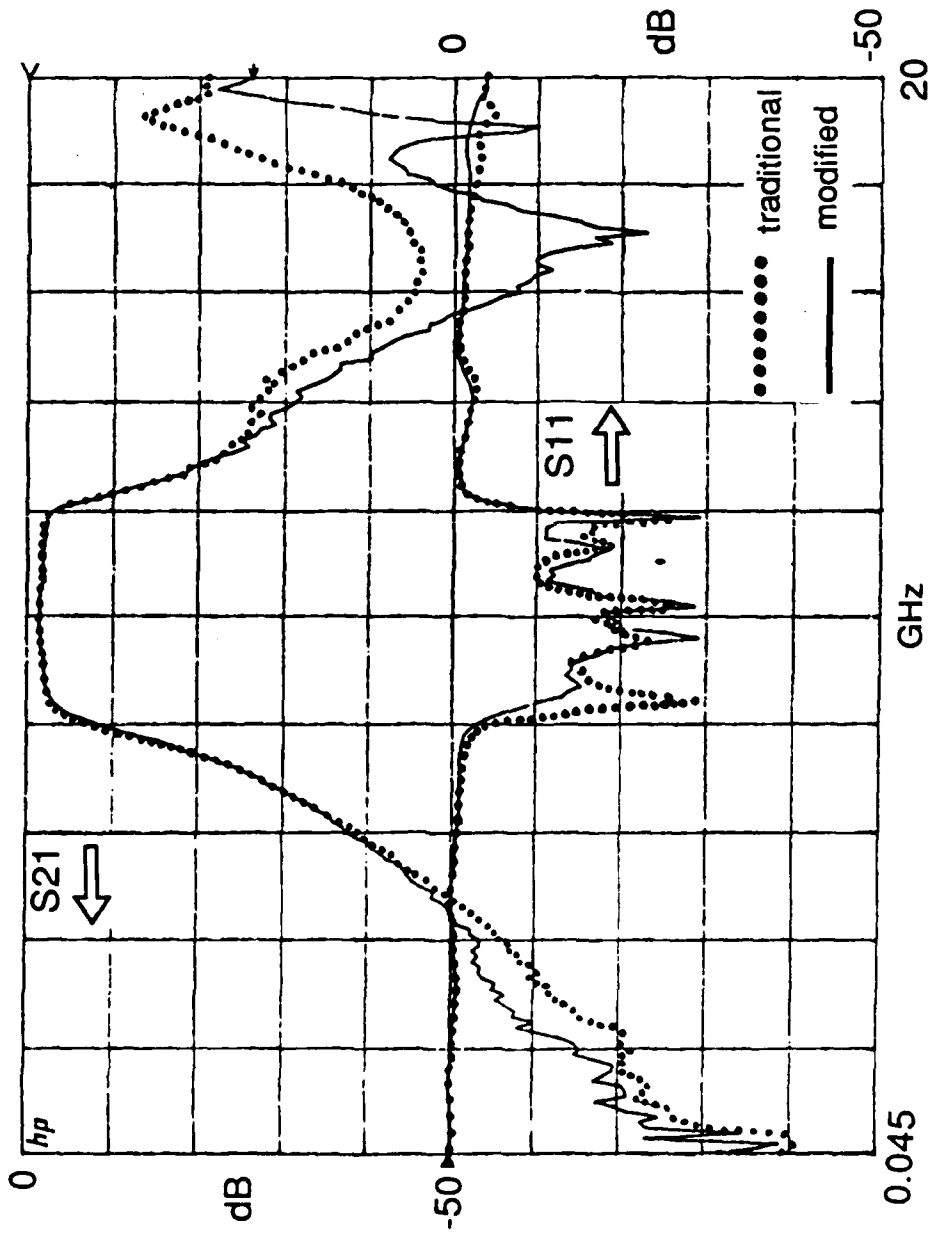

Fig. 5.10 Measured performance of filter #5.

seen that the improvement of the filters built in high dielectric constant substrate is greater than those in low dielectric constant substrate. Fig. 5.11 shows the photographs of filters #2 and #3.

The performance improvement of the modified parallel-coupled filter has been shown. Fig. 5.12 shows application of a modified filter to be an active filter. In Fig. 5.12, each tank is coupled by both adjacent tanks and a negative resistance circuit. In some coupled lines, four lines are coupled together. These four-coupled lines can not be treated in most commercial available circuit simulator. Therefore, an empirical design procedure is required. Using the structure in Fig. 5.12, the active filter may have a bandwidth of more than 40%. For an active filter with a bandwidth like this, a much wider application may be available.

In this chapter, a modified parallel-coupled filter structure was introduced. Compared to traditional parallel-coupled filter, this new filter improves the upper stopband rejection by at least 15 dB and the frequency response asymmetry phenomenon. A semi-empirical method to treat the offset microstrip gaps was outlined. Using the outlined gap model, calculated filter performance was in good agreement with measured filter performance. Based on the outlined filter structure, a broadband active filter configuration was introduced. Although the active filter design was not made in this report due to CAD problem described above, the configuration is still hopeful either waiting for a better CAD tool or by emperical design approach.

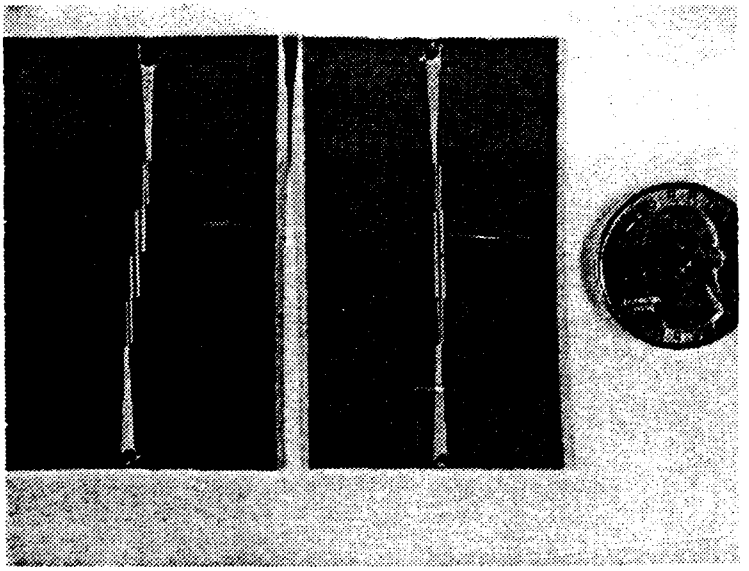

(a) The photograph of filter #2.

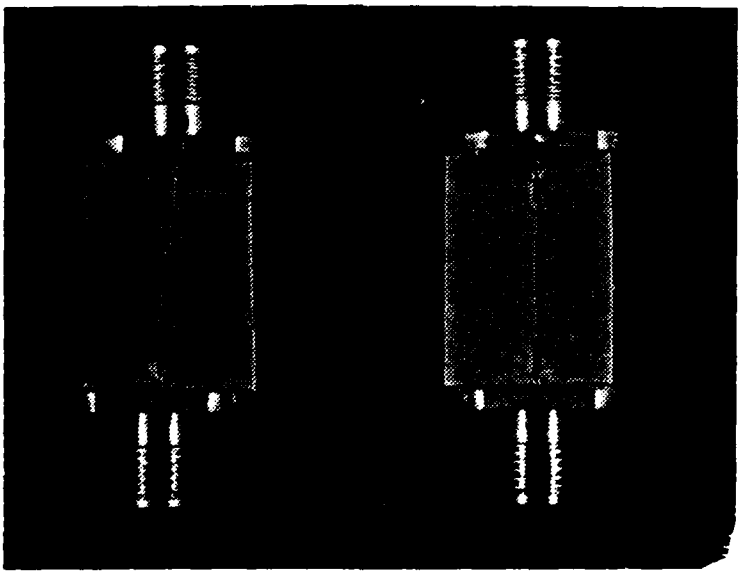

(b) The photograph of filter #3.

Fig. 5.11 The photographs of filter #2 and filter #3.

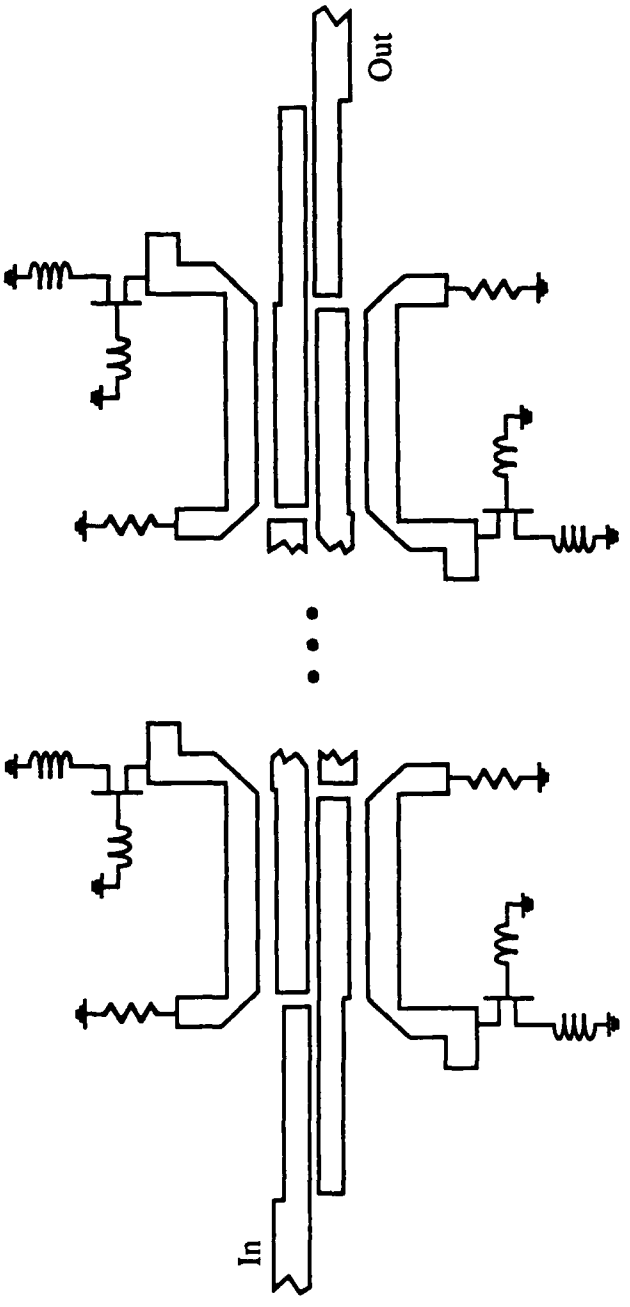

Fig. 5.12 The circuit configuration of a broadband active filter.

CHAPTER 6: TUNABLE ACTIVE FILTERS

This chapter will concentrate on the tunable active filter. Up to the present, this kind of filter circuit is mainly built using the YIG sphere. By changing the D.C. magnetic field passing through the YIG sphere, the resonant frequency of the YIG sphere is changed. A YIG-tuned filter is realized by properly coupling the YIG sphere together. Since this kind of filter is built mechanically, it is very bulky. Another disadvantage is low tuning speed due to slow varying speed of the D.C. magnetic field. The varactor is a good device for tunable filter, because varying the capacitance of a varactor is much faster than varying the applied magnetic field for the YIG sphere. If a varactor diode is placed in the tank circuit, the resonant frequency of the tank circuit will change with respect to the varactor bias voltage. This makes the filter pass band frequency tunable.

However, introducing a varactor diode into a tank circuit degrades the tank circuit Q value. Compared to the YIG sphere, the tunable tank formed by a varactor diode has a much lower Q value. The active tank circuit, therefore, is required for increasing the tank circuit Q value. Here, a varactor tuned active tank circuit is introduced as shown in Fig. 6.1. In Fig. 6.1 the varactor diode is in series with quarter-wave coupled line and quarter-wave uncoupled line. Based on the active tank circuit in Fig. 6.1, an active filter is proposed as shown in Fig. 6.2.

The varactor diode used here is Alpha DVE-6955-G device in an Alpha 30 mil 290-001 package. The varactor chip shows 2.5-3.0 pF at 0 volts and 4.25 to 1 tuning ratio. Fig. 6.3 shows the equivalent circuit of the varactor diode [23]. If

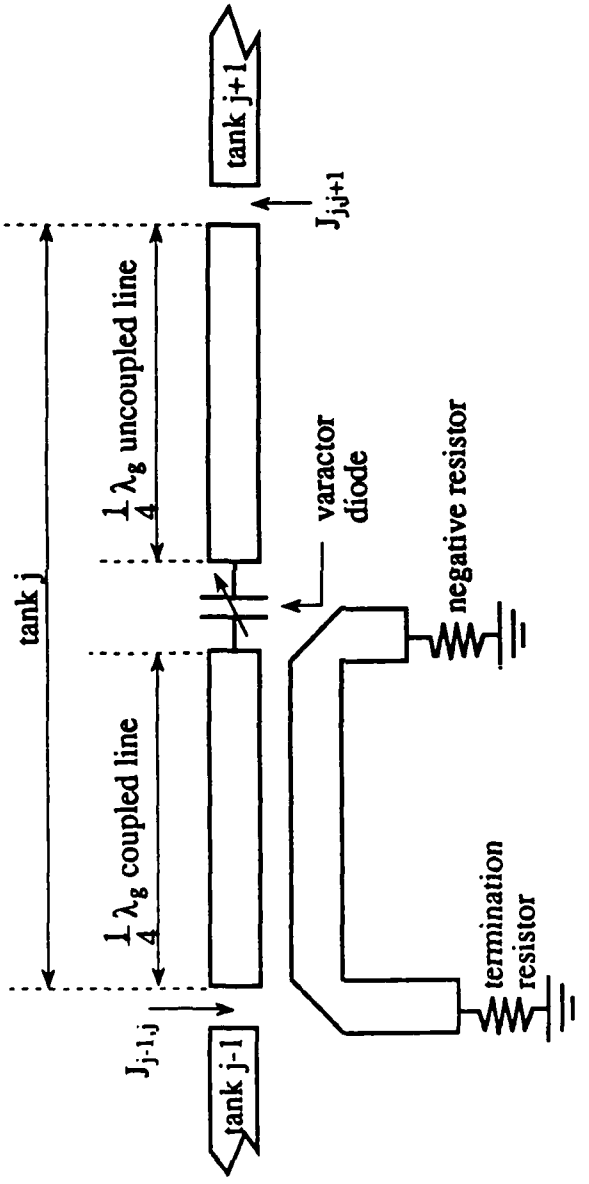

Fig. 6.1 A varactor tuned active tank circuit.

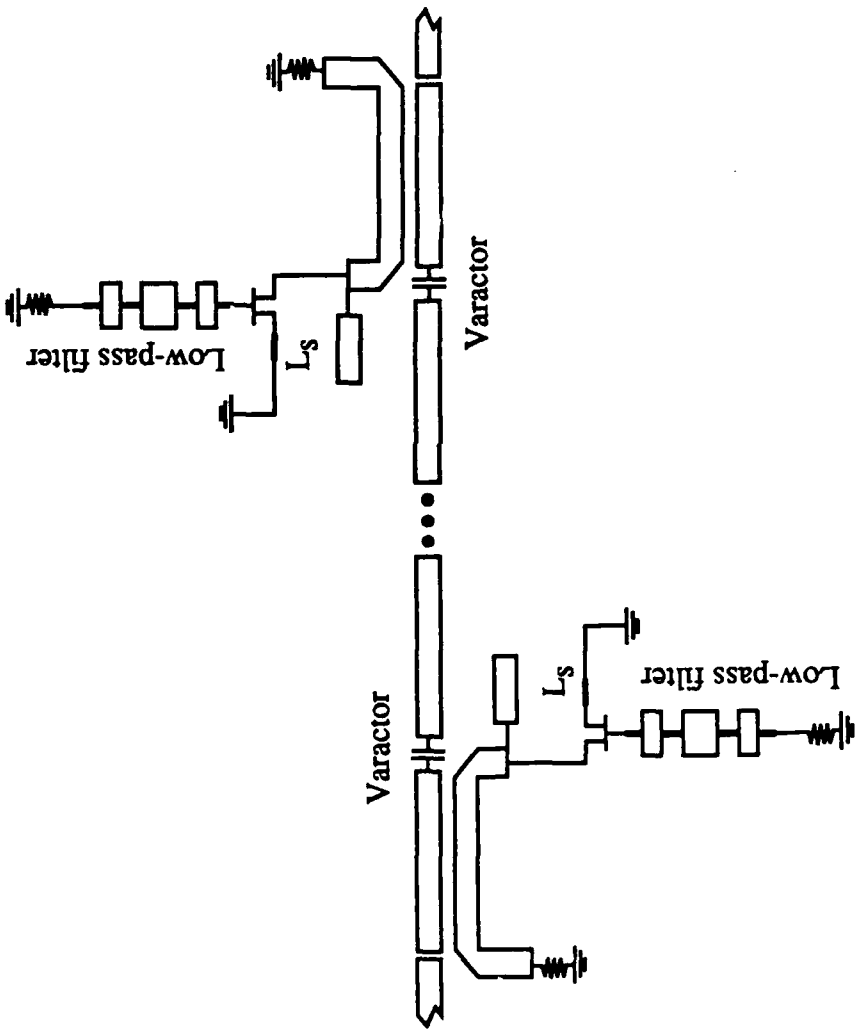

Fig. 6.2 A varactor tuned active filter.

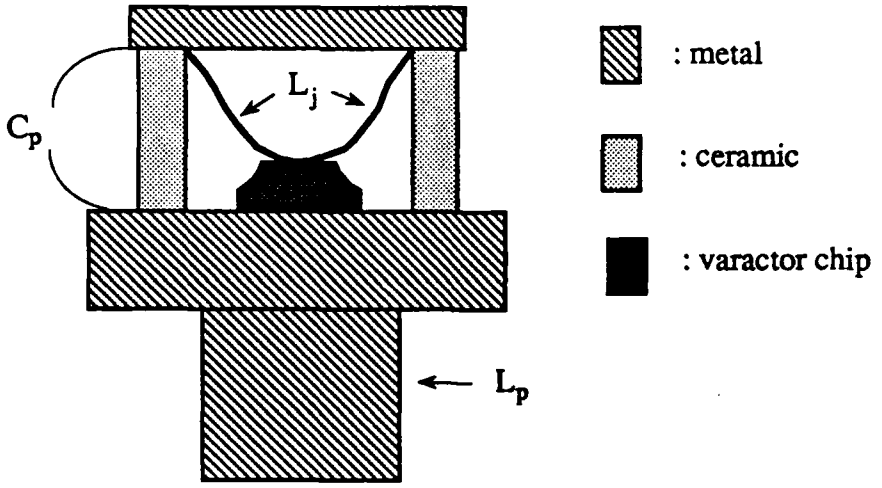

(a) The varactor diode chip in a package.

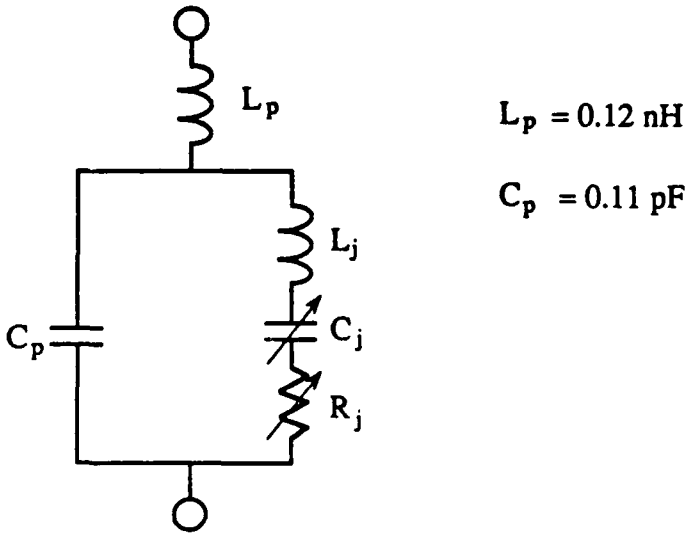

(b) The equivalent circuit of (a).

Fig. 6.3 The equivalent circuit of varactor diode.

including the package parasitic capacitance, the tuning ratio of the varactor is reduced to a value of 3.75 to 1.

Two tunable active filters were built based on the above concept. The design parameters of the filters are listed in Table. 6.1. The filters were measured by a HP-8510 network analyzer. Fig. 6.4 shows the measured one-pole tunable filter performance, and Fig. 6.5 shows the measured 2-pole tunable filter performance. Fig. 6.6 shows the calculated 2-pole tunable filter performance. Comparing Fig. 6.5 and Fig. 6.6, the results are in good agreement. Fig. 6.7 show photographs of the one-pole and 2-pole active filters. Using this packaged varactor, a tuning range of 500 MHz for the one-pole filter and 430 MHz for the 2-pole filter are obtained. If applying this circuit to MMIC, the tuning range will be broader due to elimination of the varactor package parasitics. A monolithic varactor with a tuning ratio of 15 to 1 has been reported [24]. Table 6.2 show the biasing and tuning voltages during the tuning procedure. Since the Q value of the varactor changes during the tuning procedure, the MESFET biasing voltage changes accordingly in order to compensate the different Q value of the tank. In the case of the 2-pole filter, two varactors are biased at different voltages due to the fact that the parameters of the two varactors are not identical. With carefully selected varactors, a single bias voltage for the multi-pole filter may be achieved. Another application for the MMIC tunable filter uses the Schottky contact line [25-26] or optically tuned coplanar waveguide [27-28] in place of the varactor diode. In this case, instead of a combination of lumped circuit elements (varactor) and distributed circuit elements (microstrip tank) shown in Fig. 6.1, the tank circuit may be realized in a purely distributed form.

filter type / spec.	1-pole filter	2-pole filter
center frequency	9.8-10.3 GHz	9.8-10.23 GHz
3-dB bandwidth	.15% at 9.8GHz .23% at 10.3GHz	.82% at 9.8GHz .77% at 10.23GHz
response	max. flat	Chebyshev
ripple	--	0.1 dB
substrate thickness	30 mil	30 mil
substrate dielec. const.	2.55	2.55
system * impedance	82 Ω	82 Ω
3rd order intercept. point	-7dBm at 98.GHz -5dBm at 10.3 GHz	+1dBm at 9.8GHz -2dBm at 10.23GHz

* : Non-50 Ω system impedance is tapered to 50 Ω at input and output.

Table 6.1 The filter parameters of tunable end-coupled active filter.

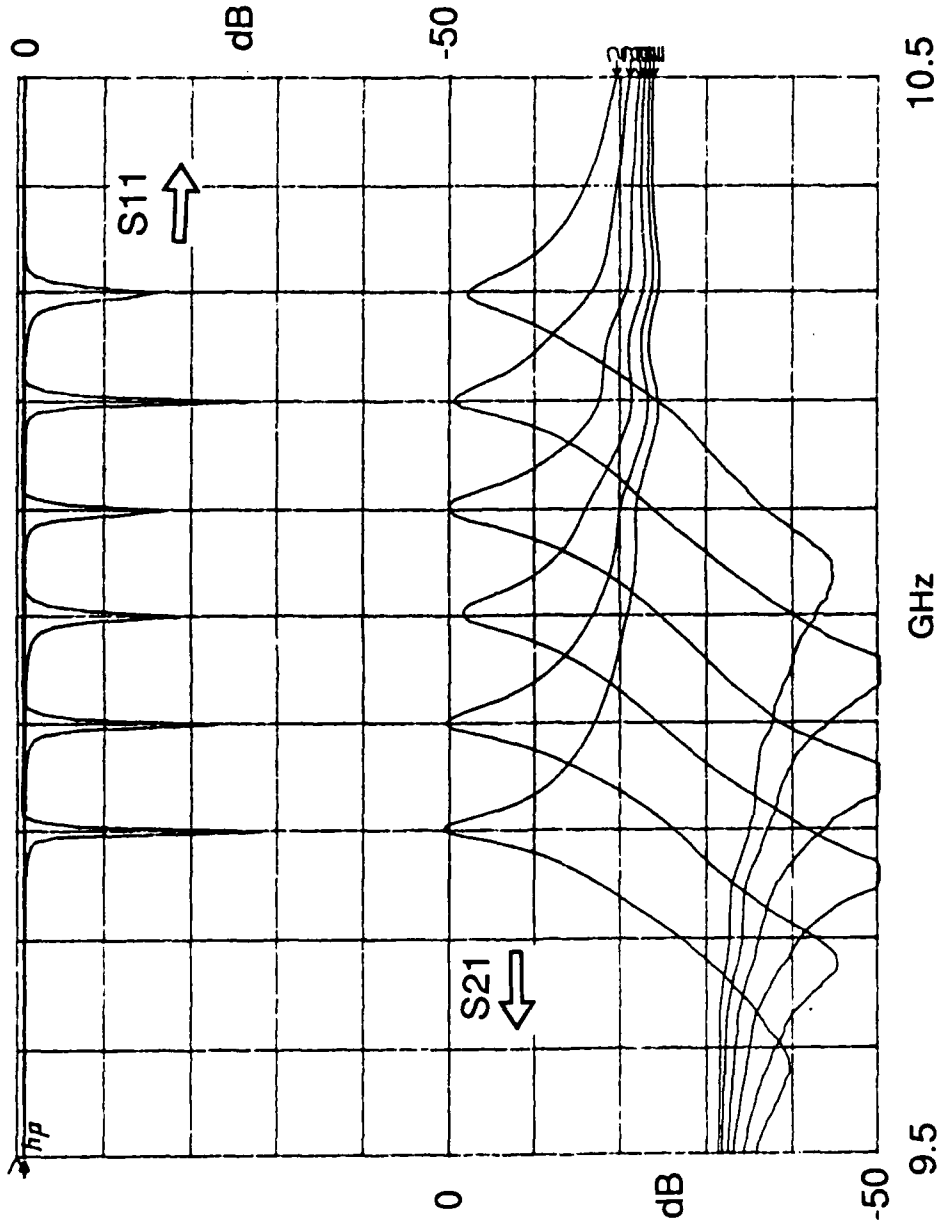

Fig. 6.4 Measured performance of the 1-pole tunable active filter.

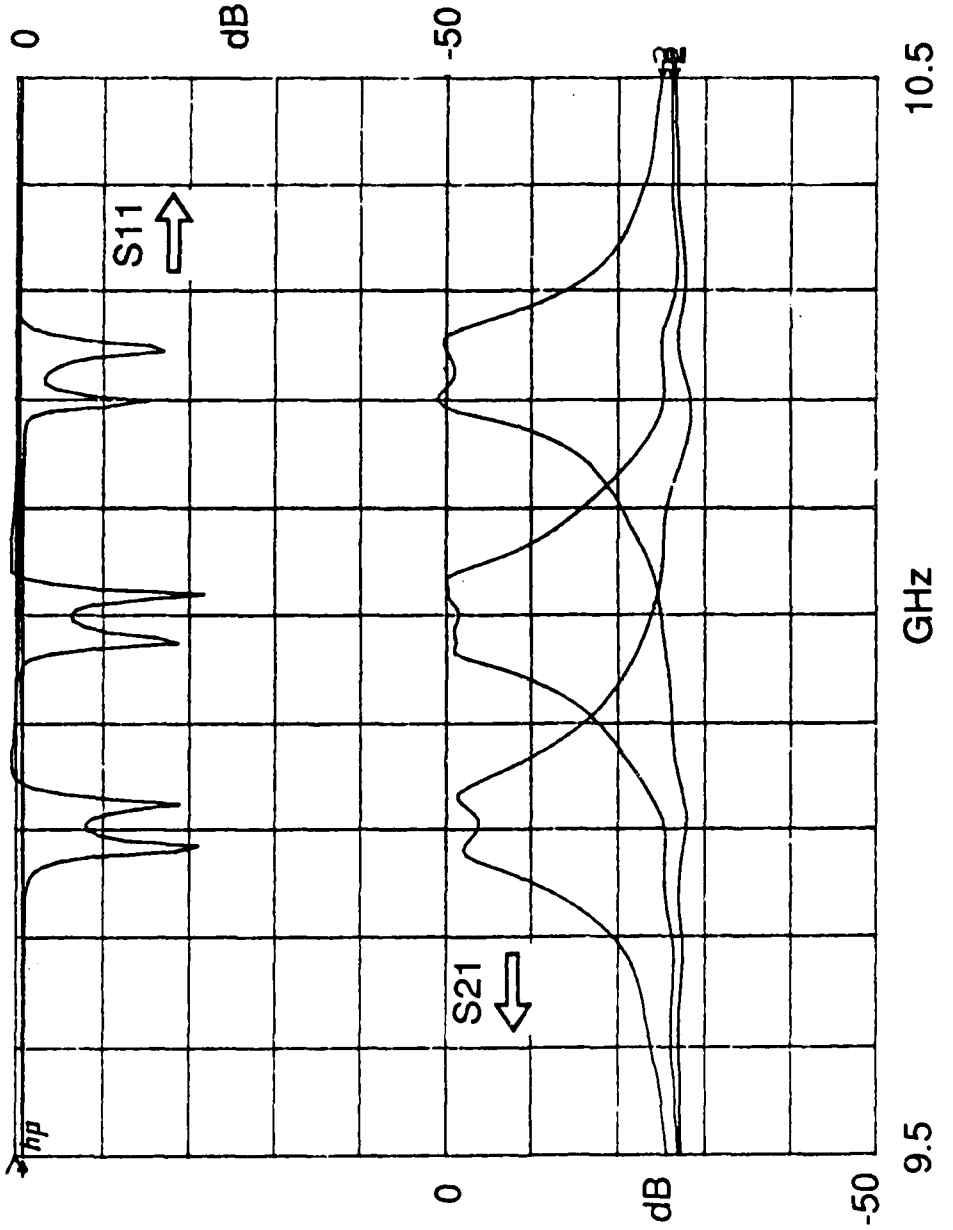

Fig. 6.5 Measured performance of the 2-pole tunable active filter.

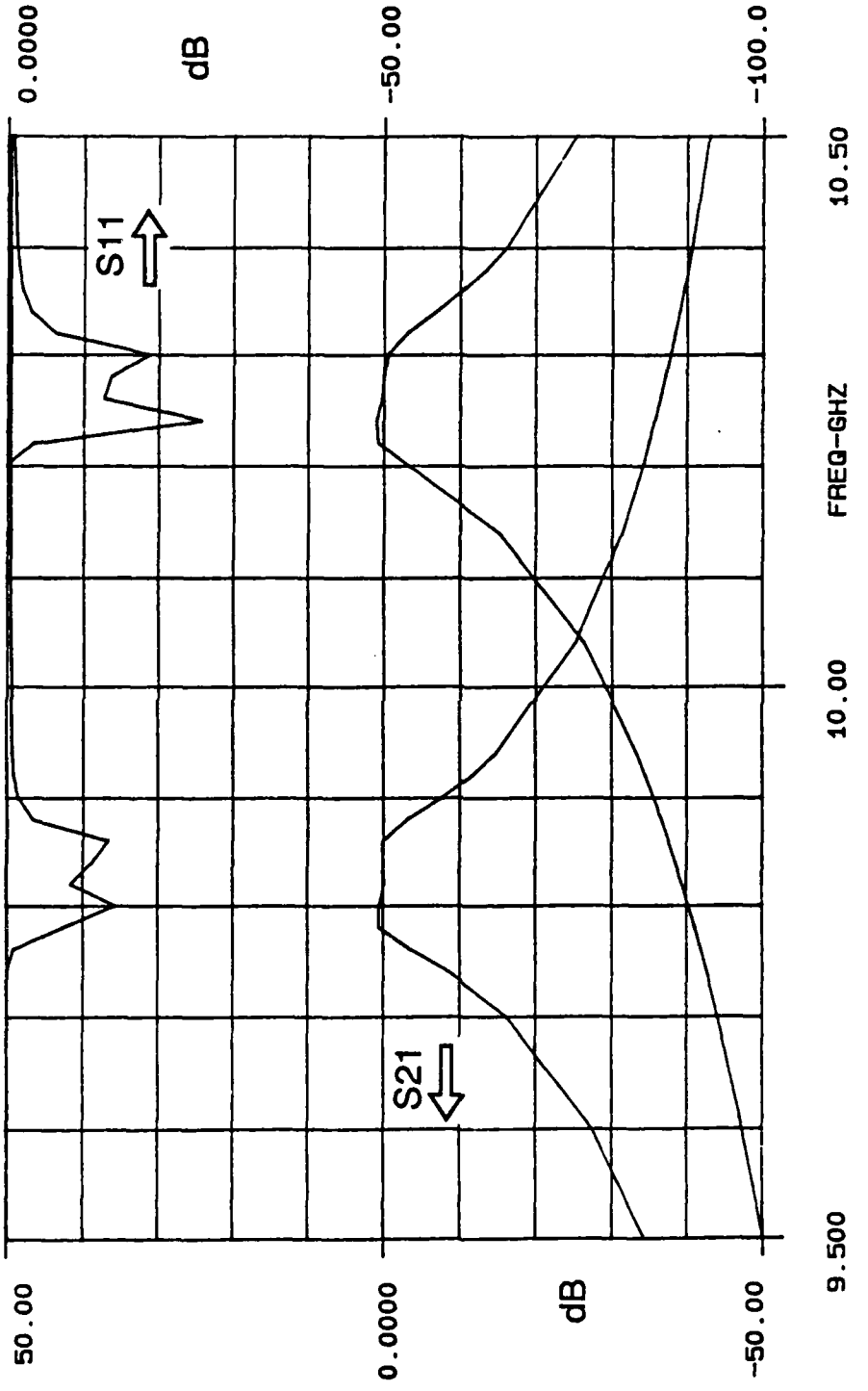

Fig. 6.6 Calculated performance of the 2-pole tunable active filter.

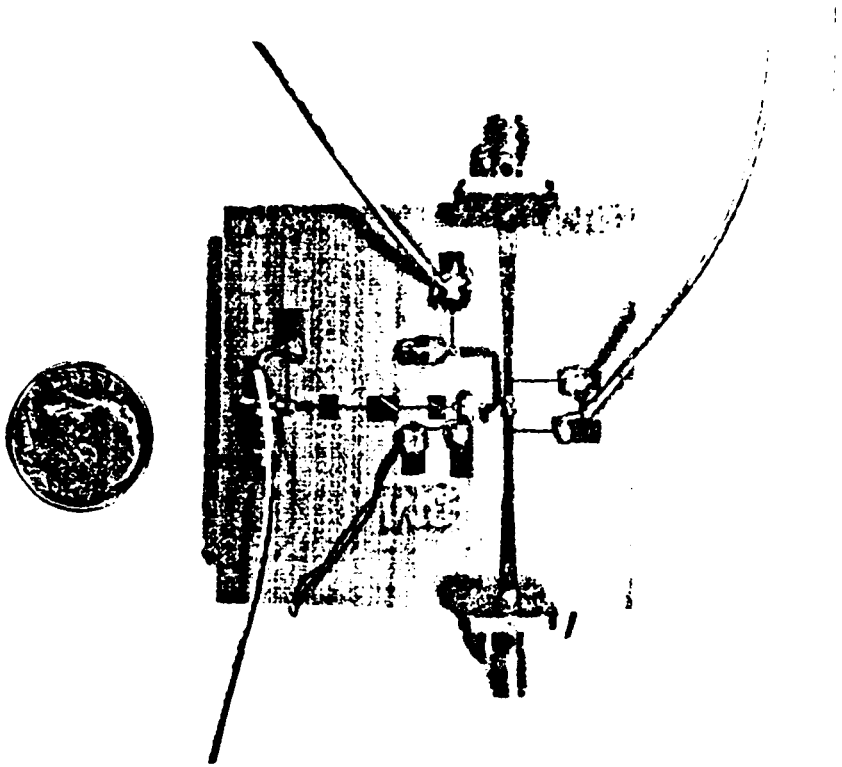

(a) The photograph of the 1-pole filter.

Fig. 6.7 The photographs of the tunable active filters.

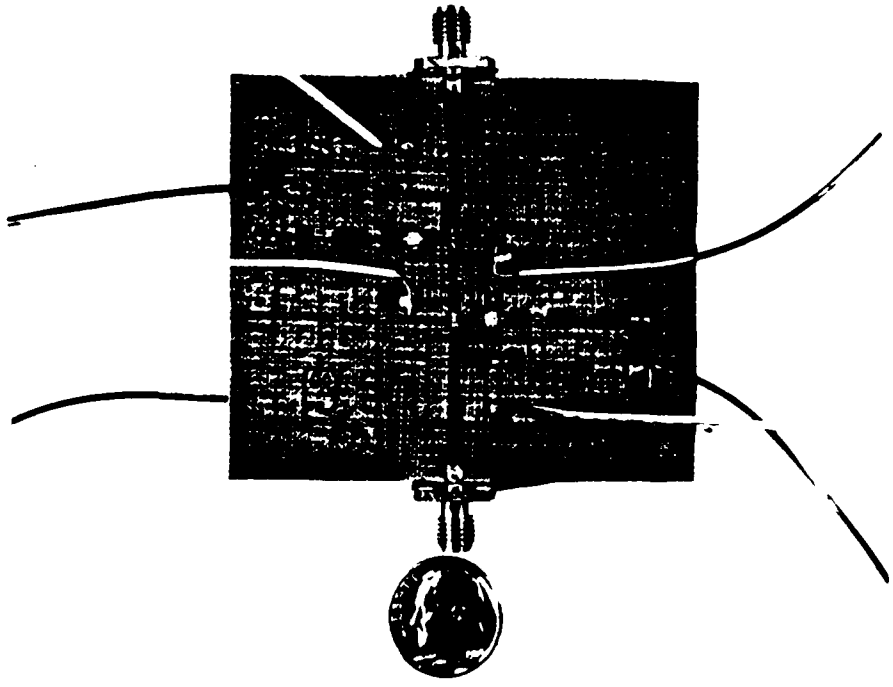

(b) The photograph of the 2-pole filter.

Fig. 6.7 The photographs of the tunable active filters.

filter type / freq.	1-pole filter gate bias = -1.14 volts		2-pole filter gate bias = -1.07 volts			
	FET drain bias	varactor bias	FET1 drain bias	FET2 drain bias	varactor1 bias	varactor2 bias
9.8 GHz	2.95 V	0 V	3.5 V	1.2 V	2.4 V	0 V
9.9 GHz	2.36 V	2 V	2.8 V	1.1 V	6.5 V	2.3 V
10.0 GHz	2.13 V	5.82 V	1.85 V	1.07 V	13.05 V	6.4 V
10.1 GHz	1.85 V	12.37 V	1.3 V	1.0 V	23.2 V	13.2 V
10.2 GHz	1.79 V	21.91 V	1.27 V	0.87 V	39.4 V	27.5 V
10.23 GHz	---	---	1.5 V	0.82 V	45 V	32.4 V
10.3 GHz	1.79 V	42 V	---	---	---	---

Table 6.2 The bias conditions for tunable filters.

In this chapter, the varactor tuned active filter was introduced. Using a packaged varactor with a tuning ratio of 3.75 to 1, two active filters were built. The measured tuning range of 500 MHz for 1-pole and 430 MHz for 2-pole filter with center frequency of 10 GHz were achieved. A broader tuning range in MMIC form was predicted. Another application for MMIC using Schottky contact line or optically tuned coplanar waveguide was introduced.

CHAPTER 7: CONCLUSIONS

In this report, a coupled negative resistance method to build an active filter has been developed. The prototype active filters are realized in microstrip form. Using different basic filter structures, the active filter may have a bandwidth from a few tenths of a percent to more than 40 percent. The design procedures for each kind of filter were outlined and can be directly used in MMIC design.

The tunable active filter was developed by introducing a varactor diode in the tank circuit. A prototype circuit shows about 500 MHz tuning range at 10 GHz. The circuit configuration is also suitable for MMIC. For MMIC, a broader tuning range was predicted.

These active filters are suitable for use in the small signal environment, for example, receiver front end, frequency preselection, frequency agile applications and so forth. The outlined circuit provides a possible way to build a MMIC filter. In the past, it was very difficult to build such kind of circuit. Therefore, full integration of a microwave subsystem has become possible.

BIBLIOGRAPHY

[1] R. A. Pucel, *Monolithic microwave integrated circuits*. New York: IEEE Press. Inc. 1985.

[2] K. D. Adams and R. Y. C. Ho, "Active filters for UHF and microwave frequencies," *IEEE Trans. Microwave Theory Tech.*, Vol. MTT-17, pp. 662-670, Sept. 1969.

[3] R. V. Snyder and D. L. Bozarth, "Analysis and Design of a microwave transistor active filter," *IEEE Trans. Microwave Theory Tech.*, Vol. MTT-18, pp. 2-9, Jan. 1970.

[4] W. Jutzi, "Microwave bandwidth active transversal filter concept with MESFETs'," *IEEE Trans. Microwave Theory Tech.*, Vol. MTT-19, pp. 760-767, Sept. 1971.

[5] C. Rauscher, "Microwave active filter based on transversal and recursive principles," *IEEE Trans. Microwave Theory Tech.*, Vol. MTT-33, pp. 1350-1360, Dec. 1985.

[6] M. Healy, R. D. Pollard and C. M. Snowden, "Active filter for MMICs," *17h European Microwave Conf. Dig.* Sept. 1987, pp. 443-447.

[7] H. Matsumura and Y. Konishi, "An active microwave filter with dielectric resonator," *IEEE MTT-S Int. Microwave Symp. Dig.*,April 1979, pp. 323-325.

[8] A. Presser, "Varactor-tunable, high-Q microwave filter," *RCA Review,* Vol. 42, pp. 691-705, Dec. 1981.

[9] G. L. Matthaei, L. Young, and E. M. T. Jones, *Microwave filters, Impedance-matching networks, and Coupling structures*. Dedham, MA: Artech House, 1980.

[10] A. B. Williams and F. J. Taylor, *Electronic Filter Design Handbook.* New York: McGraw-Hill, 1988

[11] R. E. Collin, *Foundations for microwave engineering*. New York: McGraw-Hill, 1972, ch. 7.

[12] S. B. Cohn, "Dissipating loss in multiple-coupled-resonator filters," *Proceedings of the IRE,* Vol. 47 , Aug. 1959, pp. 1342-1348.

[13] R. S. Pengelly, *Microwave field-effect transistors -- Theory, Design and Applications*. England: Research Studies Press, 1982, ch. 7.

[14] S. B. Cohn, "Direct-coupled resonator filters," *Proceedings of the. IRE,* Vol. 45, pp. 187-196, Feb. 1957.

[15] C. -Y. Chang and T. Itoh, "Narrowband planar microwave active filter," *Electronics Letters,* Vol. 25, No. 18, pp. 1228-1229, Aug. 1989.

[16] P. Benedek, and P. Silvester, "Equivalent capacitances for microstrip gaps and steps," *IEEE Trans. Microwave Theory Tech.*, Vol. MTT-20, Nov. 1972, pp. 729-733.

[17] E. Hammerstad, "Computer-aided design of microstrip couplers with accurate discontinuity models," *IEEE MTT-S Int. Microwave Symp. Dig.*, June 1981, pp. 54-56.

[18] S. B. Cohn, "Parallel-coupled transmission-line-resonator filters," *IRE Trans. Microwave Theory Tech.*, Vol MTT-6, pp. 223-231, April 1958.

[19] T. Itoh, R. Mitra, and R. D. Ward, "A method for computing edge capacitance of finite and semi-finite microstrip lines," *IEEE Trans. Microwave Theory Tech.*, Vol. MTT-20, pp. 847-849, Dec. 1972.

[20] P. Silvester and P. Benedek, "Equivalent capacitance of microstrip open circuits," *IEEE Trans. Microwave Theory Tech.*, Vol. MTT-20, pp. 511-516, Aug. 1972.

[21] R. Garge and I. J. Bahl, "Microstrip discontinuities," *Int. J. Electronics*, Vol. 45, July 1978.

[22] E. Hammerstad and Φ. Jensen, "Accurate models for microstrip computer-aided design," *IEEE MTT-S Int. Microwave Symp. Dig.*, June 1980, pp. 407-409.

[23] *Tuning Diodes,* Application Note 80500, Alpha Industries, Inc., Semiconductor Division, Woburn, MA, 1985.

[24] B. N. Scott, and G. E. Brehm, "Monolithic voltage controlled oscillator for X- and Ku- bands," *IEEE Trans. Microwave Theory Tech.*, Vol. MTT-30, pp. 2172-2177, Dec. 1982.

[25] Y. C. Shih, and T. Itoh, "Analysis of printed transmission lines for monolithic integrated circuits," *Electronics Letters,* Vol. 18, No. 14, pp. 585-586, July. 1982.

[26] C. -K. Tzuang, and T. Itoh, "Finite-element analysis of slow-wave Schottky contact printed lines," *IEEE Trans. Microwave Theory Tech.*, Vol. MTT-34, pp. 1483-1489, Dec. 1986.

[27] P. Cheung, D. P. Neikirk, and T. Itoh, "Schottky-biased, optically controlled coplanar waveguide," *IEEE MTT-S Int. Microwave Symp. Dig.*, June 1989, pp. 307-309.

[28] M. S. Islam, P. Cheung, C. -Y. Chang, D. P. Neikirk, and T. Itoh, "Optically-controlled tunable CPW resonators," to be published at *IEEE MTT-S Int. Microwave Symp. Dig.*, May 1990.